DOI:
10.2337/db16-0020

Document Version
Peer reviewed version

Hydrogen sulfide induces keap1 S-sulfhydration and suppresses diabetes-accelerated atherosclerosis via Nrf2 activation

Running title: S-sulfhydration and diabetes-accelerated atherosclerosis

Key words: S-sulfhydration; hydrogen sulfide; Nrf2; Keap1; diabetes-accelerated atherosclerosis

Liping Xie[1,2#], Yue Gu[2#], Mingliang Wen[2],Shuang Zhao[2], Wan Wang[2],Yan Ma[2], Guoliang Meng[2], Yi Han[3], Yuhui Wang[4], George Liu[4], Philip K. Moore[5], Xin Wang[6], Hong Wang[7], Zhiren Zhang[8], Ying Yu[9], Albert Ferro[10], Zhengrong Huang[1*], Yong Ji[2*]

[1]Department of Cardiology, The First Affiliated Hospital of Xiamen University, Xiamen, China; [2]Collaborative Innovation Center for Cardiovascular Disease Translational Medicine, Atherosclerosis Research Centre, Nanjing Medical University, Nanjing, China; [3]Department of Geriatrics, First Affiliated Hospital of Nanjing Medical University, Nanjing, China; [4]Institute of Cardiovascular Sciences and Key Laboratory of Molecular Cardiovascular Sciences, Ministry of Education, Peking University Health Science Center, Beijing, China; [5]Department of Pharmacology, National University of Singapore, Singapore; [6]Faculty of Life Sciences, The University of Manchester, Manchester, UK; [7]Center for Metabolic Disease Research, Department of Pharmacology, Temple University School of Medicine, Philadelphia, PA 19140, USA; [8]Third Affiliated Hospital of Harbin Medical University, Institute of Metabolic Disease, Heilongjiang Academy of Medical Science, Harbin, China; [9]Institute for Nutritional Sciences, Shanghai Institutes for Biological Sciences, Chinese

Academy of Sciences, Shanghai; [10]Department of Clinical Pharmacology, Cardiovascular Division, British Heart Foundation Centre of Research Excellence, King's College London, London, UK;

[*]Correspondence: Professor Yong Ji, Collaborative Innovation Center for Cardiovascular Disease Translational Medicine, Atherosclerosis Research Centre, Nanjing Medical University, Nanjing, 211166, China. Fax: +86 25 8686 8469; Tel: +86 25 8686 8469; e-mail: yongji@njmu.edu.cn

Doctor Zhengrong Huang, Department of Cardiology, The First Affiliated Hospital of Xiamen University, Xiamen 361003, China. Fax: +865922137558; Tel: +8613606028353; e-mail: huangzhengrong@xmu.edu.cn

[#]These authors contributed equally to this work

The total word count of the manuscript:

Figure number: 8 figures; Word count full text: 3986. Word count abstract: 195.

Online Supplement Materials included: 10 figures and 3 tables.

Abstract:

Hydrogen sulfide (H_2S) has been shown to have powerful anti-oxidative and anti-inflammatory properties which can regulate multiple cardiovascular functions. However, its precise role in diabetes-accelerated atherosclerosis remains unclear. We report here that H_2S reduced aortic atherosclerotic plaque formation with reduction in superoxide (O_2^-) generation and the adhesion molecules in streptozotocin (STZ)-induced $LDLr^{-/-}$ mice but not in $LDLr^{-/-}$ $Nrf2^{-/-}$ mice. In vitro, H_2S inhibited foam cell formation, decreased O_2^- generation, as well as increased Nrf2 nuclear translocation and consequently heme oxygenase-1 (HO-1) expression up-regulation in high-glucose (HG) plus oxidized low density lipoprotein (ox-LDL)-treated primary peritoneal macrophages from wild-type but not $Nrf2^{-/-}$ mice. H_2S also decreased O_2^- and adhesion molecules levels, increased Nrf2 nuclear translocation and HO-1 expression which were suppressed by Nrf2 knockdown in HG/ox-LDL-treated endothelial cells. H_2S increased S-sulfhydration of Keapl, induced Nrf2 dissociation from Keap1, enhanced Nrf2 nuclear translocation and inhibited O_2^- generation which were abrogated after Keapl mutated at Cys151, but not Cys273, in endothelial cells. Collectively, H_2S attenuates diabetes-accelerated atherosclerosis, which may be related to inhibition of oxidative stress via Keap1 sulfhydrylation at Cys151 to activate Nrf2 signaling. This may provide a novel therapeutic target to prevent atherosclerosis in the context of diabetes.

Introduction:

Diabetes leads to a marked increase in atherosclerosis (1). There is considerable evidence demonstrating that oxidative stress and inflammation are involved in the pathogenesis of diabetes and its complications, including atherosclerosis (2). It has been suggested that hyperglycemia-induced superoxide overproduction may be a key event in activation of pathways involved in the pathogenesis of diabetic complications (2). Approaches that limit oxidative stress may therefore translate to reduced inflammation and hence atherosclerosis.

It is well established that nuclear factor erythoid 2–related factor 2 (Nrf2) is one of the most important cellular defense mechanisms against oxidative stress. Nrf2 is broadly expressed in tissues but is only activated in response to a range of oxidative and electrophilic stimuli (3). Upon oxidative stress, Nrf2 escapes Kelch-like ECH-associated protein 1 (Keap1)-mediated repression, translocates to the nucleus, binds to antioxidant response element (ARE), and induces the expression of a battery of antioxidant proteins, one of the most important of which is heme oxygenase 1 (HO-1) (4). Nrf2 has emerged as an important target in diabetes and related complications (5,6), and low dose dh404, which is an analogue of the Nrf2 agonist bardoxolone methyl, lowers oxidative stress and protects against diabetes-associated atherosclerosis (7). These studies suggest that augmentation of antioxidant defenses via up-regulation of the Nrf2 pathway may be novel target for the prevention and treatment of diabetic complications.

Hydrogen sulfide (H_2S) plays an important role in physiology and pathophysiology in several biological systems. Emerging data suggest that H_2S improves diabetic endothelial

73 dysfunction (8), nephropathy (9), retinopathy (10), and cardiomyopathy (11). However, there
74 are no published data on the potential effect of H_2S on accelerated atherosclerosis in diabetes.

75 Some recent studies indicate that H_2S is cytoprotective during myocardial ischemia-
76 reperfusion injury in the setting of diabetes by alleviating oxidative stress, and the ability of
77 H_2S to up-regulate cellular antioxidants in the heart in a Nrf2-dependent manner (12-14). H_2S
78 may therefore play an important role in diabetes-accelerated atherosclerosis, and the effects of
79 H_2S may be mediated via activation of Nrf2. In the present study, we have characterized
80 whether and how H_2S targets on Nrf2 against the development of diabetes-accelerated
81 atherosclerosis.

Research design and Methods:

1. Animals and treatment.

LDLr$^{-/-}$ mice, on a C57BL/6 background, were purchased from Model Animal Research Center of Nanjing University. Nrf2$^{-/-}$ mice, on a C57BL/6 background, were a gift from Hongliang Li (Wuhan University), Nrf2$^{-/-}$ mice were crossed with LDLr$^{-/-}$ mice to obtain LDLr$^{-/-}$Nrf2$^{-/-}$. At ages 8 weeks, male mice were rendered diabetic by administering 60 mg/kg/day streptozotocin (STZ) intraperitoneally (i.p.) daily for 5 days. After STZ administration, diabetic mice were administered the H_2S donor GYY4137 (133 μmol/kg/day, i.p.) or vehicle, and kept on a high fat diet for 4 weeks. The dose of GYY4137 used was based on previous publications (15). Nondiabetic LDLr$^{-/-}$ or LDLr$^{-/-}$Nrf2$^{-/-}$ mice were kept on a standard chow diet for 4 weeks as control. Mice were housed (n=1/cage, n=6/group) in metabolic cages for 48h prior to metabolic analysis to acclimatise. Body weight, food intake, water intake and urinary output were determined.

All animal experiments were approved by the Committee on Animal Care of Nanjing Medical University, and were conducted according to the NIH Guidelines for the Care and Use of Laboratory Animals. All studies involving animals are reported in accordance with the ARRIVE guidelines.

2. Blood sampling.

Plasma samples were obtained from 6-h–fasted mice. Glucose was measured directly from the tail tip with a glucometer; plasma lipid levels were measured enzymatically using commercial kits (Zhong Sheng Bei Kong, Peking, China) as the manufacturer's instructions.

3. Measurement of plasma H_2S

Plasma H_2S concentration was measured as described previously (15).

4. Analysis of Atherosclerotic Lesions

To evaluate atherosclerotic lesions, en face whole and histological sections were used to analyze. The entire aorta attached to the heart was dissected and stained with Oil Red O (ORO; Sigma Aldrich, MO, USA) (16). Lesions within the sinus were visualized after staining with ORO as well as hematoxylin and eosin (HE) and quantitated as described previously (16).

5. Cell culture and experimental conditions

Mouse peritoneal macrophages were isolated from male C57BL/6 or $Nrf2^{-/-}$ mice as described previously (17). Peritoneal cells were collected by lavage and seeded in DMEM-low glucose medium (Gibco, Grand Island, USA) with 10% FBS (Gibco).

Human umbilical vein endothelial cells (HUVECs) were isolated from umbilical cords according to a previously described method (18). The endothelial cells were cultured in Endothelial Cell Medium (ECM, ScienCell, CA, USA).

EA.hy926 endothelial cells were purchased from the American Type Culture Collection (Rockville, MD, USA), and were cultured in DMEM-low glucose medium with 10% FBS.

Confluent cells (80–85%) were incubated with D-glucose (25 mM, Sigma) plus ox-LDL (50 mg/L, Yiyuan biotechnology, China), in the absence or presence of GYY4137 (50, 100 μM), sulfide-depleted GYY4137 (SDG, dissolved GYY4137 left unstoppered at room temperature for 5 days) or ZYJ1122 (a structural analogue of GYY4137 lacking sulfur) for 24 h.

6. Small interfering RNA or plasmid transfection

EA.hy926 cells were transfected with siRNA oligonucleotide against Nrf2 (sense: 5′AAGAGUAUGAGCUGGAAAAACdTdT-3′, antisense: 5′GUUUUUCCAGCUCAUACAUUCdTdT-3′, Genepharma) or negative control siRNA. HO-1 expression was silenced by HO-1 siRNA mix that was purchased from Santa Cruz. The plasmid pcDNA3-flag-Keap1 purchased from Addgene (Cambridge, MA) was termed as Keap1-WT. Single mutation at Cys-151, 273 or 288 to Ala (Haibio, Shanghai, China) was confirmed by DNA sequencing. EA.hy926 cells were transfected with expression vectors using the Lipofectamine 3000 reagent (Invitrogen).

7. Foam Cell Formation Assay

Macrophages were fixed with 4% paraformaldehyde and stained using 0.5% ORO. Images of cells were acquired using a light microscope (Nikon, Tokyo, Japan).

8. Measurement of reactive oxygen species (ROS) formation

Superoxide production in tissue sections of upper descending thoracic aorta and cells was detected by dihydroethidium (DHE) assay as the manufacturer's instructions. Briefly, cells or tissue were incubated with DHE for 30min. Fluorescence was measured with a Nikon TE2000 Inverted Microscope and quantified using Image-Pro Plus analysis software.

9. Immunofluorescence staining

Sections or cells were fixed and permeabilized, then blocked and incubated with antibody against Nrf2, VCAM-1, ICAM-1, CD31, α-SMA or Macrophage (Abcam, Cambridge, MA). After additional washing, sections or cells were incubated with directly conjugated fluorescent secondary antibodies, and with DAPI (Invitrogen). Fluorescence was imaged using a Nikon TE2000 Inverted Microscope. Positive cells and total cells were quantified in 5 different sections from 6 different mice of each genotype, using Image-Pro Plus analysis software.

10. RNA Analysis

HO-1, ICAM-1, VCAM-1, thioredoxin (Trx) and glutamate cysteine ligase catalytic subunit (GCLC) mRNA expression was quantified by real-time PCR (RT-PCR) with forward and reverse primers (Supplement Table 1).

11. Isolation of Nuclear and Cytoplasmic Proteins and Western blotting

Whole-cell, cytosolic and nuclear proteins were extracted using RIPA buffer (Sigma Aldrich) or a nuclear and cytoplasmic extraction kit (Thermo Fisher Scientific Inc.). Western Blotting was performed as described previously (19). Primary antibodies included anti-Nrf2

(Santa Cruz, MO, UAS), anti-Nrf2 (phospho S40) (Abcam), anti-HO-1 (Bioworld Technology Inc., Nanjing, China), anti-VCAM-1 (Abcam), anti-ICAM-1 (Abcam), anti-histone H3 (Bioworld), and anti-GAPDH (Abcam) antibody. Band intensities were analyzed using Image J 1.25 software.

12. Immunoprecipitation

The cells were harvested and lysed as previously described (20). Antibodies specific for Keap1 (Santa Cruz) or normal rabbit IgG were added to the supernatants followed by an incubation. Immune complexes were then precipitated with protein A-agarose beads. Bound proteins were eluted by boiling with loading buffer and analyzed by western blotting with anti-Nrf2 antibody.

13. "Tag-Switch" method

Nrf2 and Keap1 S-sulfhydration (Keap1-SSH) was detected with "Tag-Switch" method (21). The protein of Keap1 was pulled down with immunoprecipitation, and treated with biotin-linked cyanoacetate. Samples were resuspend in Laemmli buffer, heated, and subjected to western blotting analysis using anti-biotinantibody (Santa Cruz).

Statistical analysis

Data are expressed as mean ± standard error and were analyzed by one-way ANOVA followed by Newman-Keuls Multiple Comparison Test as appropriate. All statistical analyses

were performed using SPSS software, version 16.0. A value of $P<0.05$ was considered statistically significant.

Results:

1. Metabolic characteristics and plasma level of H_2S.

As expected, diabetic LDLr$^{-/-}$ mice fed a HFD had lower body weight, higher plasma total cholesterol, triacylglycerol, urinary output, water intake and food intake when compared with those fed standard chow, and these effects were unaffected by treatment with GYY4137 (Supplement Table2). Compared to LDLr$^{-/-}$ mice, plasma H_2S concentration was reduced in HFD-fed diabetic LDLr$^{-/-}$ mice which could be significantly increased by administration of GYY4137 (Supplement Table2).

2. H_2S decreases Atherosclerotic Lesions in diabetic LDLr$^{-/-}$ mice.

To determine the effect of H_2S on the formation of atherosclerotic lesions in STZ-diabetic LDLr$^{-/-}$ mice, these animals were treated with GYY4137 or vehicle for 4 weeks, and a HFD diet was used to enhance atherogenesis (Figure 1A). Initially, we measured the total aortic lesion area between the proximal ascending aorta and the bifurcation of the iliac artery by en face analysis of ORO-stained aortas. As expected, diabetic mice showed an increase in atherosclerotic plaques compared with non-diabetic control. Treatment of diabetic LDLr$^{-/-}$ mice with H_2S reduced lesion area (Figure 1B and Supplement Figure 1). Similar results were confirmed by HE and ORO staining in the aortic root (Figure 1C and 1D). Immunofluorescence analysis of sections from the aortic root revealed that macrophage content was increased in diabetic LDLr$^{-/-}$ mice, and this effect was attenuated by H_2S treatment (Figure 1E and 1F).

Collectively, these data demonstrate that exogenous H_2S decreases atherosclerotic lesions in diabetic LDLr$^{-/-}$ mice.

3. H_2S reduces the level of superoxide, VCAM-1 and ICAM-1, and activates expression of Nrf2 and associated antioxidant proteins, in vessels of diabetic LDLr$^{-/-}$ mice.

Oxidative stress plays an important role in the pathogenesis of diabetes and its complications. To determine whether the protective role of H_2S in atherosclerotic lesions might relate to reduction of ROS, we measured aortic superoxide formation by DHE assay. As expected, compared with non-diabetic LDLr$^{-/-}$ mice, endothelial fluorescence was increased in diabetic LDLr$^{-/-}$ mice. In contrast, endothelial superoxide production in diabetic LDLr$^{-/-}$ mice was attenuated following GYY4137 administration (Figure 2A and 2B). Several recent studies have identified Nrf2 as a critical transcription factor that regulates a battery of antioxidant genes in the face of oxidative stress (3). Recent work has also shown that H_2S regulates Nrf2 in myocardial tissue (12). To examine whether Nrf2 is activated in response to H_2S treatment, we investigated the intracellular localization of Nrf2. Immunofluorescence microscopy showed enhanced nuclear staining of Nrf2 in aortas of H_2S-treated in comparison to untreated diabetic LDLr$^{-/-}$ mice (Figure 2C). To further confirm the Nrf2 localization, we performed double staining for Nrf2 and CD31 (endothelial marker), α-SMA (smooth muscle cells marker) or macrophages marker and found Nrf2 could be clearly shown co-localized with three markers in aorta. And GYY4137 treatment increased Nrf2 nuclear translocation in aortic endothelial cells, smooth muscle cells and macrophages (Supplement Figure 2). In addition, the induction

of expression of the Nrf2-related antioxidant defense enzyme HO-1 was substantially increased by H_2S (Figure 2D); whilst other Nrf2 target genes, such as Trx and GCLC, were unchanged (Supplement Figure 3).

Oxidative stress induces the expression of adhesion molecules such as VCAM-1 and ICAM-1, which promote the recruitment to, and accumulation of inflammatory cells within the developing atherosclerotic lesion. Therefore, the levels of VCAM-1 and ICAM-1 in aorta were determined by RT-PCR and immunofluorescence, after 4 weeks on HFD, both VCAM-1 and ICAM-1 increased in diabetic $LDLr^{-/-}$ mice, and this effect was abrogated by treatment with H_2S (Figure 2E-2G and Supplement Figure 4). Together, these results indicate that exogenous H_2S attenuates diabetes-accelerated atherosclerosis, most likely by maintaining redox balance via the Nrf2 pathway.

4. Nrf2 deficiency abolishes the protective effects of H_2S in STZ-induced $LDLr^{-/-}$ mice.

To further explore the pathophysiological significance of H_2S-induced Nrf2 activation *in vivo*, we mated $LDLr^{-/-}$ mice with $Nrf2^{-/-}$ mice to generate $LDLr^{-/-}Nrf2^{-/-}$ mice. After injection of STZ and 4 weeks of HFD, with or without concomitant GYY4137 treatment, metabolic characteristics were assessed (Supplement Table 3). Histological assessment of atherosclerotic lesions at the aortic sinus by ORO and HE staining showed a marked increase of plaques in the aortic root from $LDLr^{-/-}Nrf2^{-/-}$ diabetic mice fed HFD, and the aortic plaque area was now not reduced by H_2S treatment (Figure 3A and 3B). Moreover, the expression of superoxide, VCAM-1, and ICAM-1 were not reduced after treatment of GYY4137 in diabetic $LDLr^{-/-}Nrf2^{-}$

$^{-/-}$ mice (Figure 3C-G and Supplement Figure 5). Complementary analyses of Nrf2 target gene levels in aorta revealed that the expression of HO-1 could not be augmented by H_2S in the presence of Nrf2 deficiency (Figure 3H). These results demonstrate that Nrf2 is necessary for the inhibitory effect of H_2S to be exerted on diabetes-accelerated atherosclerosis *in vivo*.

5. H_2S decreases foam cell formation and production of superoxide, and enhances HO-1 expression via activation of Nrf2, in HG plus ox-LDL treated mouse macrophages.

Accumulation of cholesterol and cholesteryl esters in macrophages and subsequent foam cell formation is a critical early event in atherogenesis. To further investigate the molecular mechanisms underlying the effects of H_2S, we established a macrophage model in hyperglycaemic and hyperlipidemic conditions *in vitro*, which replicates some of the characteristics of macrophages in the diabetes-accelerated atherosclerotic mouse model. Mouse peritoneal macrophages from C57BL/6 were incubated with HG plus ox-LDL, with or without GYY4137 for 24 h; following which foam cell formation and ROS production were measured by ORO staining and DHE assay respectively. As expected, foam cell formation was induced in macrophages exposed to ox-LDL, and this effect was exaggerated by co-incubation with HG (data not shown). Pretreatment with GYY4137 (50 or 100 μM), but not SDG or ZYJ1122, abrogated this effect (Figure 4A and Supplement Figure 6). In addition, superoxide generation was enhanced in HG plus ox-LDL-stimulated macrophages (Figure 4B and 4C), and this too was attenuated by pretreatment with H_2S.

Next, to test whether Nrf2 is involved in the effects of H_2S on macrophage function, we investigated its intracellular localization. Immunofluorescence microscopy showed enhanced nuclear staining of Nrf2 in cells treated with H_2S in comparison to vehicle-treated cells, in the presence of HG plus ox-LDL (Figure 4D). Western blotting analysis of cytoplasmic and nuclear protein extracts also indicated increased nuclear accumulation of Nrf2 protein in cells treated with H_2S (Figure 4E and 4F), suggesting that Nrf2 is activated in response to H_2S exposure. Similarly, in the presence of HG plus ox-LDL, H_2S-pretreated macrophages exhibited increased production of HO-1 (Figure 4G).

Additional experiments were performed to confirm the involvement of Nrf2 in the protective effect of H_2S, using mouse peritoneal macrophages isolated from $Nrf2^{-/-}$ mice. Inhibition of foam cell formation and superoxide generation induced by HG plus ox-LDL was attenuated by H_2S treatment in Nrf2 knockout (KO) cells (Figure 5A-5C). Consistent with these results, elevation of HO-1 expression by H_2S treatment was also abolished in the Nrf2 KO group (Figure 5D). Furthermore, HO-1 knockdown by siRNA or inhibition by ZnPP (HO-1 inhibitor) also abrogated H_2S-mediated suppression of O_2^- generation and foam cell formation (Supplement Figure 7). These results demonstrate that Nrf2/HO-1 pathway is responsible for the inhibitory effects of H_2S on HG plus ox-LDL-induced foam cell formation and oxidative stress in macrophages.

6. H_2S decreases ROS, ICAM-1 and VCAM-1 generation, and enhances HO-1 expression via Nrf2 signaling, in HG plus ox-LDL treated endothelial cells.

It has been reported that endothelial dysfunction caused by lipotoxicity or hyperglycemia is mediated through several mechanisms including increased oxidative stress and proinflammatory responses. Therefore, we measured the effect of H_2S on oxidative stress in endothelial cells by DHE assay. Stimulation of HUVECs with HG plus ox-LDL for 24 h caused an increase in production of superoxide, and this increase was alleviated by pretreatment with GYY4137 (50 or 100 μM) (Figure 6A and 6B) but not with SDG or ZYJ1122 (Supplement Figure 8).

To confirm whether the cytoprotective effect of H_2S against oxidative stress was also associated with Nrf2, we carried out immunofluorescence and western blotting for Nrf2. GYY4137 had no effect on Nrf2 phosphorylation, but can increase the Nrf2 protein expression in the nuclear in HG plus ox-LDL-stimulated endothelial cells (Figure 6C-E and Supplement Figure 9A), implying that H_2S may promote phosphorylation-independent Nrf2 nuclear translocation. Consistent with our *in vivo* study, H_2S reduced the expression of VCAM-1 and ICAM-1 (Figure 6F and 6G); in addition, the Nrf2 target gene HO-1 was also increased by H_2S pretreatment (Figure 6H and 6I). To further clarify whether H_2S-induced down-regulation of oxidative stress was dependent on activation of the Nrf2 pathway, EA.hy926 cells were transfected Nrf2 siRNA for 24 h before H_2S and HG+ox-LDL treatment. Western blotting revealed that individual transfection with Nrf2 siRNA successfully reduced Nrf2 protein expression at 24 h post-transfection, as compared to negative control siRNA-transfected (Ctl siRNA) cells (Figure 7A). Nrf2 knockdown abrogated H_2S-mediated suppression of ROS

294 production induced by HG plus ox-LDL in endothelial cells (Figure 7B and 7C). Furthermore,
295 inhibition of HO-1 expression or activity by siRNA or ZnPP abolished the protective effects of
296 H_2S (Supplement Figure 10). Together, these results indicate that the anti-oxidative and anti-
297 inflammatory effects of H_2S in the presence of HG plus ox-LDL are partially mediated by
298 Nrf2/HO-1 pathway in endothelial cells.

299 **7. H_2S S-sulfhydrylated Keapl at Cys151 to regulate Nrf2 activity and reduce ROS**
300 **generation in HG plus ox-LDL treated endothelial cells.**

301 Generally, Nrf2 is retained in an unactivated state binding with Keap1 in the cytoplasm,
302 which serves as an adaptor for the degradation of Nrf2. Nrf2 can be activated by physiological
303 stimuli which disrupt Keap1-Nrf2 interactions leading to nuclear translocation of Nrf2 (22). To
304 further explore the mechanisms of Nrf2 activation, we immunoprecipitated the cell lysate using
305 an anti-Keap1 antibody and blotted for Nrf2. The results showed that GYY4137 decreased
306 Nrf2/Keap1 interaction in HG plus ox-LDL-treated endothelial cells (Figure 8A). S-
307 sulfhydration, the addition of one sulfhydryl to thiol side of cysteine residue and formation of
308 persulfide group (R-S-S-H), has been identified as a novel post-translational modification by
309 H_2S in eukaryotic cells. However, the covalent modification in sulfhydration is reversed by
310 reducing agents, such as dithiothreitol (DTT) (23). We tested the S-sulfhydration of Nrf2 and
311 found that H_2S donor GYY4137 or NaHS had no effect on Nrf2 S-sulfhydration (Supplement
312 Figure 9B).We next investigated whether H_2S directly modified Keapl. After preincubation
313 with GYY4137, EA.hy926 cells were treated with HG plus ox-LDL and subjected to "Tag-

Switch" assay. There was stronger S-sulfhydration of Keap1 after GYY4137 incubation (Figure 8B). To identify the S-sulfhydrated cysteine residue, Keap1 mutated at Cys151, Cys273, or Cys288 to alanine (C151A, C273A, or C288A) or wild-type (WT) was transfected into endothelial cells. H_2S still enhanced S-sulfhydration on Keap1 after wild-type or mutated Keap1 at Cys288 but not at Cys151 and Cys273 overexpression (Figure 8C). H_2S increased Nrf2 dissociation from Keap1 in HG plus ox-LDL-treated endothelial cells after Keap1-WT and Keap1-C273A but not Keap1-C151A overexpression (Figure 8D). Moreover, after Keap1 mutation at Cys151, H_2S failed to induce Nrf2 nuclear translocation or decrease the generation of superoxide (Figure 8E-G). These findings indicate that S-sulfhydration of Cys151 in Keap1 is critical for Nrf2 activation in HG plus ox-LDL treated endothelial cells.

Discussion:

A complex interaction between inflammation, lipid deposition, monocytic infiltration and endothelial dysfunction is responsible for the initiation and progression of diabetes-accelerated atherosclerosis (1). Experimental evidence for an anti-atherosclerotic effect of H_2S has been obtained in numerous studies in hyperlipidemic animal and cell models (15, 24-26), but the anti-atherosclerotic effect in the context of diabetes has not been previously investigated. Recent data published by our group demonstrated that treatment with H_2S decreased aortic atherosclerotic plaque formation and partially restored aortic endothelium-dependent relaxation in ApoE$^{-/-}$ mice fed with a HFD (15). Exogenous H_2S improved endothelium-dependent relaxation in isolated vascular rings incubated with high glucose, and attenuated hyperglycemia-induced DNA injury and improved cellular viability in bEnd.3 microvascular endothelial cells (8). These data suggested that exogenous H_2S might serve as a treatment option for diabetic-associated atherosclerosis. Indeed, in the present study, we found that H_2S supplementation reduces lesion area and macrophage infiltration in diabetic LDLr$^{-/-}$ mice. In agreement with these findings, we also observed that H_2S treatment attenuated HG+ox-LDL-induced foam cell formation. Our study provides the first evidence that H_2S may prevent development of diabetes-accelerated atherosclerosis, and that this does not relate to any effects on circulating blood glucose or cholesterol.

Several pathological mechanisms have been proposed for diabetic vascular complications, including diabetes-accelerated atherosclerosis, such as increased polyol pathway flux,

increased advanced glycation end-product formation and activation of protein kinase C; all of these, in association with hyperglycemia-induced ROS accumulation (27). Endothelial cells and macrophages are both sources of ROS. Indeed, in our study, we have demonstrated that STZ-treated LDLr$^{-/-}$ mice fed a HFD showed an increase in atherosclerotic plaques compared with non-diabetic LDLr$^{-/-}$ mice, accompanied by increased superoxide production in aorta and this was further confirmed in HG plus ox-LDL-treated macrophages and endothelial cells. The increase in ROS promotes the recruitment and accumulation of inflammatory cells to the developing atherosclerotic lesion. H_2S has also been shown to have powerful antioxidant properties. Exogenous H_2S attenuates the hyperglycemia-induced enhancement of ROS formation in endothelial cells and human U937 monocytes (8,28). In line with these findings, we observed that H_2S decreased superoxide generation in macrophages and endothelial cells cultured with HG plus ox-LDL. Furthermore, we showed that superoxide production in the aortas of diabetic LDLr$^{-/-}$ mice was reduced following H_2S administration. In this study, we show for the first time that inhibition of HG+ox-LDL-generated ROS with H_2S prevents the diabetes-induced increase in plaque area. Additionally, we found that H_2S attenuates the increase in aortic VCAM-1 and ICAM-1 expression.

Recent studies indicate that H_2S may up-regulate endogenous antioxidants through an Nrf2-dependent signaling pathway (12) to combat oxidative stress. To date, the role of Nrf2 in atherosclerosis remains controversial. Myeloid Nrf2 deficiency aggravates both early and late stages of atherosclerosis in LDLr$^{-/-}$ mice (29,30). Ellagic acid improves oxidant-induced

endothelial dysfunction and atherosclerosis partly via Nrf2 activation (31). In contrast to these reported protective actions, Nrf2 has also been ascribed as having potentially pro-atherogenic functions, in that $ApoE^{-/-}Nrf2^{-/-}$ double knockout mice exhibited reduced plaque (32). In diabetes-associated atherosclerosis, a novel analog of the Nrf2 agonist bardoxolone methyl, has been found to reduce atherosclerotic lesions as well as oxidative stress and the proinflammatory mediators ICAM-1 and VCAM-1, in STZ-induced diabetic $ApoE^{-/-}$ mice (7). Our data support previous findings as regards the protective actions of Nrf2, and suggest that H_2S can attenuate endothelial dysfunction, foam cell formation and atherosclerosis in the context of diabetes, at least partially via the Nrf2/HO-1 pathway.

A widely accepted model for Nrf2 nuclear accumulation describes that a modification of the Keap1 cysteines leads directly to the dissociation of the Keap1-Nrf2 complex (33). Recently, one study suggested that Keap1 can be S-sulfhydrated at Cys151 which stimulates the dissociation of Nrf2 to enable its translocation to nucleus (34). We found that Keap1 could be S-sulfhydrated at Cys151 and Cys273 simultaneously, but only the S-sulfhydration of Cys151 was involved in activation of Nrf2 which decreased the ROS generation to improve endothelial function. Kim S et al. found that thiol modification of Keap1 Cys288 is responsible for daillyl trisulfide-induced activation of Nrf2 signaling (35). However, in our study, Cys288 of Keap1 could not be S-sulfhydrated after treatment with GYY4137. This discrepancy may be attributed to different regulatory mechanisms in different cell types, the use of different H_2S treatment regiments giving rise to different kinetics of H_2S release. Nevertheless, this study demonstrates

384 a significant role of Keap1 Cys151 S-sulfhydration in the protective effects of H_2S against
385 diabetes-accelerated atherosclerosis.

386 In summary, our study provided definitive evidence that H_2S can lessen diabetes-
387 accelerated atherosclerosis in $LDLr^{-/-}$ mice and improve hyperglycemia/ox-LDL-induced injury
388 in macrophages and endothelial cells. This protective effect of H_2S can partly be attributed to
389 activation of Nrf2 via Keap1 S-sulfhydration at Cys151. Our findings suggest that activation of
390 Nrf2 may be a potential novel therapeutic strategy against diabetes-associated vascular disease,
391 and that exogenous H_2S administration in the form of an H_2S donor GYY4137 may be of
392 therapeutic benefit in the setting of diabetes-associated atherosclerosis. Finally, our study
393 provides new insight into the mechanisms responsible for the anti-atherosclerotic effects of H_2S
394 in the context of diabetes.

Author Contributions.

L.X. and Y.G. researched data, contributed to discussion, and edited the manuscript. W.M., S.Z., W.W. and Y.M. researched data. G.M. contributed to discussion and proof-read the manuscript. H.F., Y.H., and Y.W. researched data. G.L. designed study and reviewed data. P.K.M., X.W., H.W., Z.Z. and Y.Y. reviewed the manuscript. A.F. contributed to discussion and re-wrote the manuscript. Z.H. reviewed data and edited the manuscript. Y.J. designed study, reviewed data and edited manuscript. All authors have approved the final version of the manuscript. Prof. Y.J. is the guarantor of this work and, as such, had full access to all the data in the study and takes responsibility for the integrity of the data and the accuracy of the data analysis.

Acknowledgments

We gratefully acknowledge Prof. Hongliang Li (Renmin Hospital of Wuhan University, Wuhan University) to offer the $Nrf2^{-/-}$ mice. This work was supported by grants from the National Natural Science Foundation of China (grant nos. 81200197, 81170083, 81330004), the National Basic Research Program of China (973) (grant no 2011CB503903, 2012CB517803). The authors declare no financial conflict of interest that might be construed to influence the results or interpretation of their manuscript.

References:

1. Eckel RH, Wassef M, Chait A, Sobel B, Barrett E, King G, Lopes-Virella M, Reusch J, Ruderman N, Steiner G, Vlassara H: Prevention Conference VI: Diabetes and Cardiovascular Disease: Writing Group II: pathogenesis of atherosclerosis in diabetes. *Circulation* 105:e138-e143, 2002

2. Forbes JM, Cooper ME: Mechanisms of diabetic complications. *Physiol Rev* 93:137-188, 2013

3. Ma Q: Role of nrf2 in oxidative stress and toxicity. *Annu Rev Pharmacol Toxicol* 53:401-426, 2013

4. Niture SK, Khatri R, Jaiswal AK: Regulation of Nrf2-an update. *Free Radic Biol Med* 66:36-44, 2014

5. Xu X, Luo P, Wang Y, Cui Y, Miao L: Nuclear factor (erythroid-derived 2)-like 2 (NFE2L2) is a novel therapeutic target for diabetic complications. *J Int Med Res* 41:13-19, 2013

6. Ramprasath T, Selvam GS: Potential impact of genetic variants in Nrf2 regulated antioxidant genes and risk prediction of diabetes and associated cardiac complications. *Curr Med Chem* 20:4680-4693, 2013

7. Tan SM, Sharma A, Stefanovic N, Yuen DY, Karagiannis TC, Meyer C, Ward KW, Cooper ME, de Haan JB: Derivative of bardoxolone methyl, dh404, in an inverse dose-dependent manner lessens diabetes-associated atherosclerosis and improves diabetic kidney disease. *Diabetes* 63:3091-3103, 2014

8. Suzuki K, Olah G, Modis K, Coletta C, Kulp G, Gero D, Szoleczky P, Chang T, Zhou Z, Wu L, Wang R, Papapetropoulos A, Szabo C: Hydrogen sulfide replacement therapy protects the vascular endothelium in hyperglycemia by preserving mitochondrial function. *Proc Natl Acad Sci U S A* 108:13829-13834, 2011

9. Zhou X, Feng Y, Zhan Z, Chen J: Hydrogen sulfide alleviates diabetic nephropathy in a streptozotocin-induced diabetic rat model. *J Biol Chem* 289:28827-28834, 2014

10. Si YF, Wang J, Guan J, Zhou L, Sheng Y, Zhao J: Treatment with hydrogen sulfide alleviates streptozotocin-induced diabetic retinopathy in rats. *Br J Pharmacol* 169:619-631, 2013

11. Zhou X, An G, Lu X: Hydrogen sulfide attenuates the development of diabetic cardiomyopathy. *Clin Sci (Lond)* 128:325-335, 2015

12. Calvert JW, Jha S, Gundewar S, Elrod JW, Ramachandran A, Pattillo CB, Kevil CG, Lefer DJ: Hydrogen sulfide mediates cardioprotection through Nrf2 signaling. *Circ Res* 105:365-374,

2009

13. Peake BF, Nicholson CK, Lambert JP, Hood RL, Amin H, Amin S, Calvert JW: Hydrogen sulfide preconditions the db/db diabetic mouse heart against ischemia-reperfusion injury by activating Nrf2 signaling in an Erk-dependent manner. *Am J Physiol Heart Circ Physiol* 304:H1215-H1224, 2013

14. Zhou X, An G, Chen J: Inhibitory effects of hydrogen sulphide on pulmonary fibrosis in smoking rats via attenuation of oxidative stress and inflammation. *J Cell Mol Med* 18:1098-1103, 2014

15. Liu Z, Han Y, Li L, Lu H, Meng G, Li X, Shirhan M, Peh MT, Xie L, Zhou S, Wang X, Chen Q, Dai W, Tan CH, Pan S, Moore PK, Ji Y: The hydrogen sulfide donor, GYY4137, exhibits anti-atherosclerotic activity in high fat fed apolipoprotein E(-/-) mice. *Br J Pharmacol* 169:1795-1809, 2013

16. Cheng WL, Wang PX, Wang T, Zhang Y, Du C, Li H, Ji Y: Regulator of G-protein signalling 5 protects against atherosclerosis in apolipoprotein E-deficient mice. *Br J Pharmacol*, 2014

17. Mauldin JP, Srinivasan S, Mulya A, Gebre A, Parks JS, Daugherty A, Hedrick CC: Reduction in ABCG1 in Type 2 diabetic mice increases macrophage foam cell formation. *J Biol Chem* 281:21216-21224, 2006

18. Ferro A, Queen LR, Priest RM, Xu B, Ritter JM, Poston L, Ward JP: Activation of nitric oxide synthase by beta 2-adrenoceptors in human umbilical vein endothelium in vitro. *Br J Pharmacol* 126:1872-1880, 1999

19. Xie L, Liu Z, Lu H, Zhang W, Mi Q, Li X, Tang Y, Chen Q, Ferro A, Ji Y: Pyridoxine inhibits endothelial NOS uncoupling induced by oxidized low-density lipoprotein via the PKCalpha signalling pathway in human umbilical vein endothelial cells. *Br J Pharmacol* 165:754-764, 2012

20. Mi Q, Chen N, Shaifta Y, Xie L, Lu H, Liu Z, Chen Q, Hamid C, Becker S, Ji Y, Ferro A: Activation of endothelial nitric oxide synthase is dependent on its interaction with globular actin in human umbilical vein endothelial cells. *J Mol Cell Cardiol* 51:419-427, 2011

21. Park CM, Macinkovic I, Filipovic MR, Xian M: Use of the "tag-switch" method for the detection of protein S-sulfhydration. *Methods Enzymol* 555:39-56, 2015

22. Zhang DD, Lo SC, Sun Z, Habib GM, Lieberman MW, Hannink M: Ubiquitination of Keap1, a BTB-Kelch substrate adaptor protein for Cul3, targets Keap1 for degradation by a proteasome-independent pathway. *J Biol Chem* 280:30091-30099, 2005

480 23. Mustafa AK, Gadalla MM, Sen N, Kim S, Mu W, Gazi SK, Barrow RK, Yang G, Wang R,
481 Snyder SH: H2S signals through protein S-sulfhydration. *Sci Signal* 2:a72, 2009

482 24. Mani S, Li H, Untereiner A, Wu L, Yang G, Austin RC, Dickhout JG, Lhotak S, Meng QH,
483 Wang R: Decreased endogenous production of hydrogen sulfide accelerates atherosclerosis.
484 *Circulation* 127:2523-2534, 2013

485 25. Wang XH, Wang F, You SJ, Cao YJ, Cao LD, Han Q, Liu CF, Hu LF: Dysregulation of
486 cystathionine gamma-lyase (CSE)/hydrogen sulfide pathway contributes to ox-LDL-induced
487 inflammation in macrophage. *Cell Signal* 25:2255-2262, 2013

488 26. Wang Y, Zhao X, Jin H, Wei H, Li W, Bu D, Tang X, Ren Y, Tang C, Du J: Role of
489 hydrogen sulfide in the development of atherosclerotic lesions in apolipoprotein E knockout
490 mice. *Arterioscler Thromb Vasc Biol* 29:173-179, 2009

491 27. Brownlee M: Biochemistry and molecular cell biology of diabetic complications. *Nature*
492 414:813-820, 2001

493 28. Manna P, Jain SK: L-cysteine and hydrogen sulfide increase PIP3 and AMPK/PPARgamma
494 expression and decrease ROS and vascular inflammation markers in high glucose treated
495 human U937 monocytes. *J Cell Biochem* 114:2334-2345, 2013

496 29. Collins AR, Gupte AA, Ji R, Ramirez MR, Minze LJ, Liu JZ, Arredondo M, Ren Y, Deng
497 T, Wang J, Lyon CJ, Hsueh WA: Myeloid deletion of nuclear factor erythroid 2-related factor
498 2 increases atherosclerosis and liver injury. *Arterioscler Thromb Vasc Biol* 32:2839-2846, 2012

499 30. Ruotsalainen AK, Inkala M, Partanen ME, Lappalainen JP, Kansanen E, Makinen PI,
500 Heinonen SE, Laitinen HM, Heikkila J, Vatanen T, Horkko S, Yamamoto M, Yla-Herttuala S,
501 Jauhiainen M, Levonen AL: The absence of macrophage Nrf2 promotes early atherogenesis.
502 *Cardiovasc Res* 98:107-115, 2013

503 31. Ding Y, Zhang B, Zhou K, Chen M, Wang M, Jia Y, Song Y, Li Y, Wen A: Dietary ellagic
504 acid improves oxidant-induced endothelial dysfunction and atherosclerosis: role of Nrf2
505 activation. *Int J Cardiol* 175:508-514, 2014

506 32. Barajas B, Che N, Yin F, Rowshanrad A, Orozco LD, Gong KW, Wang X, Castellani LW,
507 Reue K, Lusis AJ, Araujo JA: NF-E2-related factor 2 promotes atherosclerosis by effects on
508 plasma lipoproteins and cholesterol transport that overshadow antioxidant protection.
509 *Arterioscler Thromb Vasc Biol* 31:58-66, 2011

510 33. Holland R, Fishbein JC: Chemistry of the cysteine sensors in Kelch-like ECH-associated
511 protein 1. *Antioxid Redox Signal* 13:1749-1761, 2010

512 34. Yang G, Zhao K, Ju Y, Mani S, Cao Q, Puukila S, Khaper N, Wu L, Wang R: Hydrogen

sulfide protects against cellular senescence via S-sulfhydration of Keap1 and activation of Nrf2. *Antioxid Redox Signal* 18:1906-1919, 2013

35. Kim S, Lee HG, Park SA, Kundu JK, Keum YS, Cha YN, Na HK, Surh YJ: Keap1 cysteine 288 as a potential target for diallyl trisulfide-induced Nrf2 activation. *PLoS One* 9:e85984, 2014

519 **Figure Legends**

520 **Figure 1. Effects of H_2S on atherosclerosis in HFD fed diabetic LDLr$^{-/-}$ mice.** Diabetic
521 LDLr$^{-/-}$ mice were fed a high-fat diet (HFD) and received daily ip injection of saline or H_2S
522 donor GYY4137 (133 μmol/kg/day) for 4 weeks. **A**, Schema of experimental procedure. **B**,
523 Lesion areas shown was quantified using Oil-Red O (ORO) staining of the thoracoabdominal
524 aorta. **C** and **D**, Representative ORO and hematoxylin eosin (HE)-stained images and
525 quantification of aortic sinus sections from LDLr$^{-/-}$ (n=6), STZ+HFD (n=9) and
526 STZ+HFD+GYY4137 (n=8). Scale bars, 200 μm. **E** and **F**, Frozen sections of aortic root were
527 stained for anti-macrophage (green) and DAPI (blue). Dotted lines indicate the boundary of
528 lesion and aortic tunica intima. L indicates lumen. Quantitative data in the graph represent the
529 positively stained area percentage of plaque (n=6). Scale bars, 100 μm. Data shown are
530 mean±SEM. ***P<0.001 vs. LDLr$^{-/-}$ mice. $^{###}$P<0.001 vs. STZ+HFD mice.

531 **Figure 2. Effects of H_2S on ROS formation, Nrf2, VCAM-1 and ICAM-1 expression in**
532 **aortas from HFD fed diabetic LDLr$^{-/-}$ mice. A**, Representative dihydroethidium (DHE)
533 fluorescence image of aortic tissue from LDLr$^{-/-}$, STZ+HFD and STZ+HFD+GYY4137. Scale
534 bars, 100 μm. **B**, Quantification of DHE fluorescence image of A, ***P<0.001 vs. LDLr$^{-/-}$ mice.
535 $^{##}$P<0.01 vs. STZ+HFD mice, n=6. **C**, Representative immunostaining for Nrf2 (green) and
536 DAPI (blue) of aorta. Scale bars, 50 μm. **D**, mRNA levels of HO-1 in the aortas of LDLr$^{-/-}$ (n=6),
537 STZ+HFD (n=6) and STZ+HFD+GYY4137 (n=8), as determined by real-time quantitative
538 polymerase chain reaction (RT-PCR) analysis. **E** and **F**, mRNA levels of VCAM-1 and ICAM-

1 in the aortas of LDLr$^{-/-}$ (n=6), STZ+HFD (n=6) and STZ+HFD+GYY4137 (n=6). **G**, Representative VCAM-1 and ICAM-1 immunostaining of aortic arch section (with arrows). Scale bars, 100 μm. *P<0.05, **P<0.01 and ***P<0.001 vs. LDLr$^{-/-}$ mice. $^{\#}$P<0.05, $^{\#\#}$P<0.01 vs. STZ+HFD mice. ROS indicates reactive oxygen species; Nrf2, nuclear factor E2-related factor 2; VCAM-1, vascular cell adhesion molecule-1; ICAM-1, intercellular adhesion molecule-1.

Figure 3. Effects of H_2S on diabetes-accelerated atherosclerosis in LDLr$^{-/-}$Nrf2$^{-/-}$ mice. Diabetic LDLr$^{-/-}$Nrf2$^{-/-}$ mice were fed a HFD and received daily ip injection of saline or GYY4137 (133 μmol/kg/day) for 4 weeks. **A** and **B**, Representative ORO and HE-staining images and quantification of aortic sinus sections from LDLr$^{-/-}$Nrf2$^{-/-}$ mice, STZ+HFD and STZ+HFD+GYY4137 (n=5). Scale bars, 200 μm. **C**, Representative DHE fluorescence image of aorta. Scale bars, 100 μm. **D**, Quantification of DHE fluorescence image of C, *P<0.05, ***P<0.001 vs. LDLr$^{-/-}$ mice, $^{\#\#}$P<0.01, $^{\#\#\#}$P<0.001 vs. LDLr$^{-/-}$Nrf2$^{-/-}$ mice, n=5-7. **E,** Representative VCAM-1 and ICAM-1 immunostaining of aortic arch section (with arrows). Scale bars, 100 μm. **F** and **G,** mRNA levels of VCAM-1 and ICAM-1 in the aorta of LDLr$^{-/-}$ Nrf2$^{-/-}$, STZ+HFD and STZ+HFD+GYY4137 (n=5). **H,** mRNA levels of HO-1 in the aorta (n=5). Data shown are mean±SEM. *P<0.05, **P<0.01 vs. control. HO-1 indicates heme oxygenase-1.

Figure 4. Effects of H_2S on HG plus ox-LDL-treated primary peritoneal macrophages. Isolated peritoneal macrophages from C57BL/6 mice were treated with D-glucose (25 mM) plus ox-LDL (50 mg/L) in the presence or absence of GYY4137 (50 or 100 μM) for 24 h. **A**,

559 Macrophages incubated as above and stained with ORO. Scale bars, 20 μm. **B**, Representative
560 DHE stained images showing ROS generation in each condition. Scale bars, 50 μm. **C**,
561 Quantification of DHE fluorescence image of B, $^{**}P<0.01$ vs. untreated control. $^{\#}P<0.05$,
562 $^{\#\#}P<0.01$ vs. treatment with HG plus ox-LDL, n=5. **D**, Immunohistochemistry was performed
563 on macrophages stained with antibody directed against Nrf2 (green) and DAPI (blue). Scale
564 bars, 20 μm. **E** and **F**, Western blotting analysis and quantification of cytoplasmic and nuclear
565 Nrf2 protein. GAPDH and histone H3 were used for normalization for cytoplasmic and nuclear
566 proteins respectively (n=4). **G**, Western blotting analysis and quantification of HO-1 protein
567 expression (n=4). Data shown are mean±SEM. $^{*}P<0.05$, $^{**}P<0.01$ and $^{***}P<0.001$ vs. untreated
568 control. $^{\#\#}P<0.01$ vs. treatment with HG plus ox-LDL.

569 **Figure 5. Effects of H_2S on HG plus ox-LDL-treated primary peritoneal macrophages**
570 **from Nrf2$^{-/-}$ mice.** Isolated peritoneal macrophages from C57BL/6 (wild-type, WT) and Nrf2^{-}
571 $^{/-}$ mice were treated with D-glucose (25 mM) plus ox-LDL (50 mg/L) in the presence or absence
572 of GYY4137 (100 μM) for 24 h. **A**, macrophages from Nrf2$^{-/-}$ mice were stained with ORO.
573 Scale bars, 20 μm. **B**, Representative DHE stained images of macrophages from WT and Nrf2^{-}
574 $^{/-}$ mice. Scale bars, 50 μm. **C**, Quantification of DHE fluorescence image of B, $^{***}P<0.001$ vs.
575 WT control. $^{\#\#\#}P<0.001$ vs. WT with HG plus ox-LDL. $^{\&\&\&}P<0.001$ vs. Nrf2$^{-/-}$ control. n=3. **D**,
576 Western blotting analysis and quantification of HO-1 protein expression in macrophages from
577 Nrf2$^{-/-}$ mice (n=4). Data shown are mean±SEM. $^{*}P<0.05$ vs. untreated control.

578 **Figure 6. Effects of H_2S on HG plus ox-LDL-treated endothelial cells.** HUVECs were
579 treated with D-glucose (25 mM) plus ox-LDL (50 mg/L) in the presence or absence of
580 GYY4137 (50 or 100 μM) for 24 h. **A**, Representative DHE stained images showing ROS
581 generation. Scale bars, 100 μm. **B**, Quantification of DHE fluorescence image of A, $^{**}P<0.01$
582 vs. untreated control. $^{\#}P<0.05$, $^{\#\#}P<0.01$ vs. treatment with HG plus ox-LDL. n=5. **C**,
583 Immunohistochemistry was performed on HUVECs stained with antibody directed against
584 Nrf2 (green) and DAPI (blue). Scale bars, 20 μm. **D** and **E**, Western blotting analysis and
585 quantification of cytoplasmic and nuclear Nrf2 protein. GAPDH and histone H3 were used for
586 normalization for cytoplasmic (n=5) and nuclear (n=4) proteins respectively. **F** and **G**, Western
587 blotting analysis and quantification of VCAM-1 (n=4) and ICAM-1 (n=3) protein. **H**, mRNA
588 levels of HO-1 (n=5). **I**, Western blotting analysis and quantification of HO-1 protein
589 expression (n=4). Data shown are mean±SEM. $^{*}P<0.05$, $^{**}P<0.01$ and $^{***}P<0.001$ vs. untreated
590 control. $^{\#}P<0.05$, $^{\#\#}P<0.01$ and $^{\#\#\#}P<0.001$ vs. treatment with D-glucose plus ox-LDL. HUVECs
591 indicates human umbilical vein endothelial cells.

592 **Figure 7. Effects of H_2S on HG plus ox-LDL-treated Nrf2 knockdown endothelial cells.**
593 EA.hy926 endothelial cells were transfected with control siRNA (Ctl siRNA) or Nrf2 siRNA
594 for 24 h and then treated with D-glucose (25 mM) and ox-LDL (50 mg/L) in the presence or
595 absence of GYY4137 (100 μM) for 24 h. **A,** Western blotting analysis and quantification of
596 Nrf2 (n=3). Data shown are mean±SEM. $^{***}P<0.001$ vs. Ctl siRNA control. B, Representative
597 DHE staining images. Scale bars, 50 μm. **C**, Quantification of DHE fluorescence image of B,

598 $^{**}P<0.01$, vs. Ctl siRNA control. $^{\#}P<0.05$ vs. Ctl siRNA with HG plus ox-LDL. $^{\&\&\&}P<0.001$ vs.

599 Nrf2 siRNA control, n=5.

600 **Figure 8. H_2S S-sulfhydrylated Keap1 at Cys151 to regulate Nrf2 transcription activity**

601 **and reduce the generation of ROS in HG plus ox-LDL-treated endothelial cells. A**,

602 EA.hy926 endothelia cells were treated with GYY4137 (100 μM) followed by D-glucose (25

603 mM) plus ox-LDL (50 mg/L) stimulation for 24 h, cell lysates were immunoprecipitated with

604 an anti-Keap1 or an anti-IgG antibody (negative control), and blotted with an anti-Nrf2

605 antibody (upper panel). An aliquot of total lysate was analyzed for Keap1, Nrf2 and GAPDH

606 expression (lower panels). **B**, EA.hy926 endothelial cells were treated with DTT (1 mM,

607 negative control） or D-glucose (25 mM) plus ox-LDL (50 mg/L) in the presence or absence of

608 GYY4137 (100 μM) for 2 h. S-sulfhydration on Keap1 was detected with "Tag-Switch" method.

609 **C**, After plasmid transfection of wild type Keap1(Keap1-WT) or mutated Keap1 at Cys151,

610 Cys273, Cys288 for 24 h followed by GYY4137 (100 μM) treated for another 2 h, S-

611 sulfhydration on Keap1 was detected with "Tag-Switch" method. **D**, Transfected cells were

612 treated with D-glucose (25 mM) plus ox-LDL (50 mg/L) in the presence or absence of

613 GYY4137 (100 μM) for another 24 h, cell lysates immunoprecipitated with an anti-Keap1

614 antibody and the immunoprecipitated proteins were subjected to immunoblot analysis with anti-

615 Nrf2 antibodies (upper panels). The total lysates was analyzed with anti-Keap1, anti-Nrf2, and

616 anti-GAPDH antibodies (lower panels). **E** and **F**, Transfected cells treated with D-glucose (25

617 mM) plus ox-LDL (50 mg/L) in the presence or absence of GYY4137 (100 μM) for 24h.

Nuclear extracts prepared from cells were subjected to western blotting analysis for detecting the nuclear localization of Nrf2 (n=4). ROS accumulation was determined by the DHE assay. Scale bars, 50 μm. Data shown are mean±SEM. $^{**}P<0.01$ vs. Keap1-WT transfected cells treatment with D-glucose plus ox-LDL. **G**, Quantification of DHE fluorescence image of F, $^{**}P<0.01$ vs. untreated Keap1-WT transfected cells. $^{\#\#}P<0.01$ vs. Keap1-WT transfected cells treated with D-glucose and ox-LDL. $^{\&\&}P<0.01$ vs. untreated C151A transfected cells, n=4.

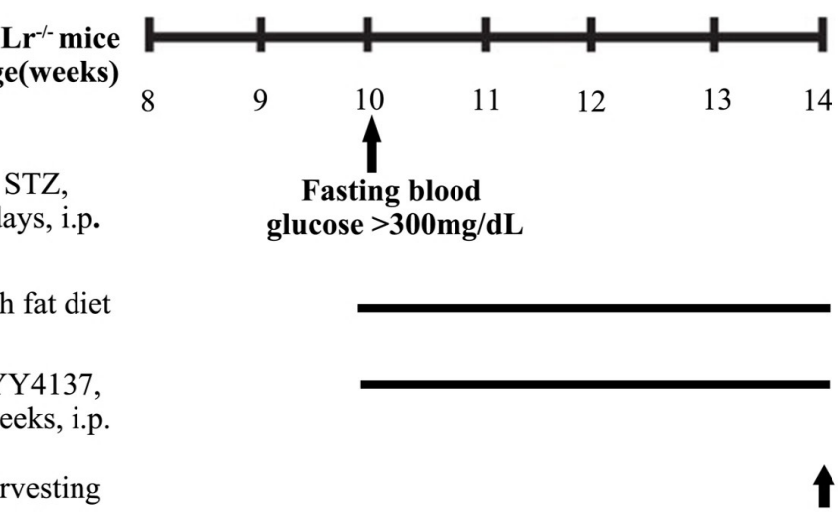
Lr-/- mice
ge(weeks)
8
9
10
11
12
13
14
STZ,
lays, i.p.
Fasting blood
glucose >300mg/dL
h fat diet
YY4137,
eeks, i.p.
rvesting

B

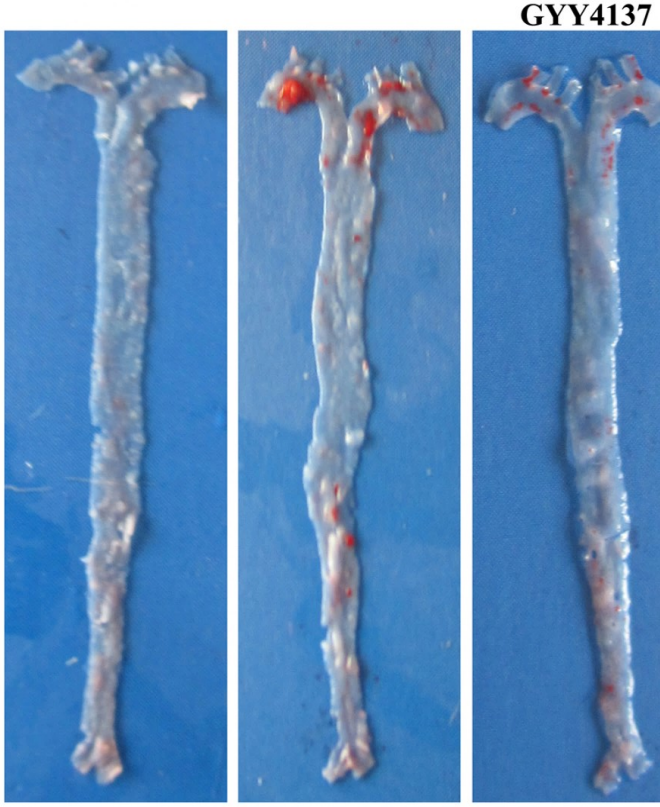
LDLr-/-
STZ+HFD
STZ+HFD+
GYY4137

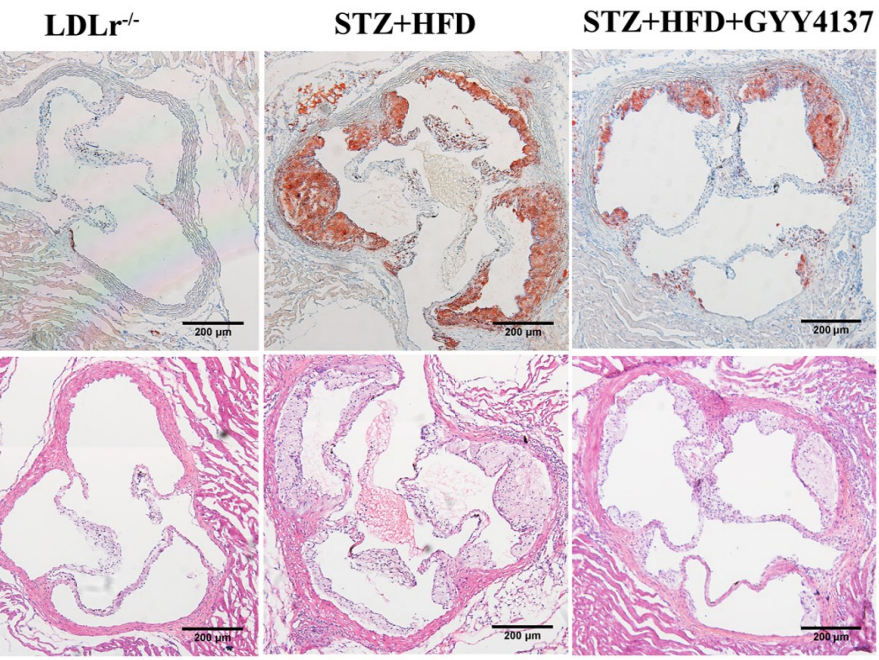
LDLr-/-
STZ+HFD
STZ+HFD+GYY4137
200 μm

D

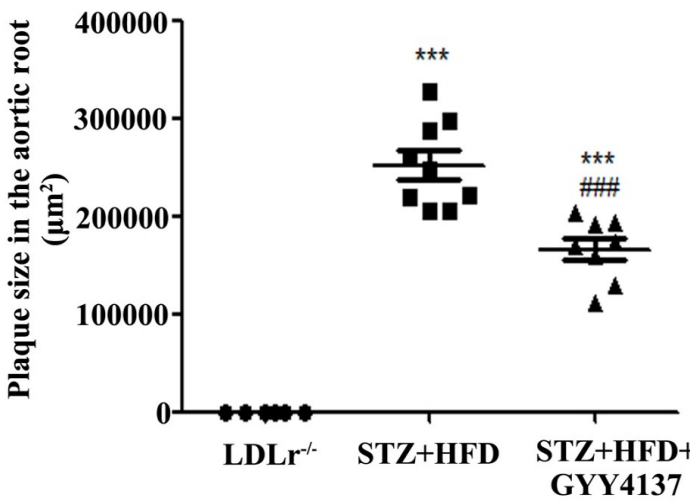
Plaque size in the aortic root
(μm2)
400000
300000
200000
100000
0
***
***
###
LDLr-/-
STZ+HFD
STZ+HFD+
GYY4137

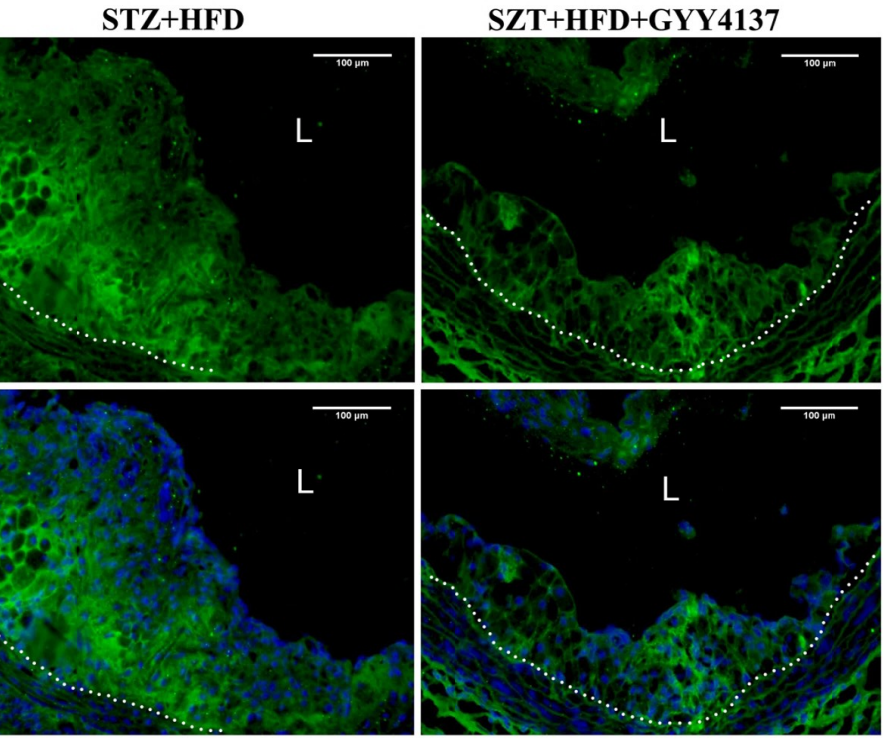
STZ+HFD
SZT+HFD+GYY4137
100 μm
L

F

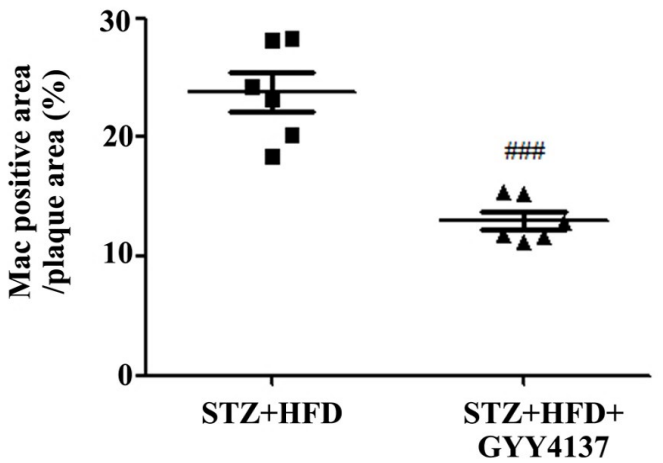
Mac positive area
/plaque area (%)
30
20
10
0
###
STZ+HFD
STZ+HFD+
GYY4137

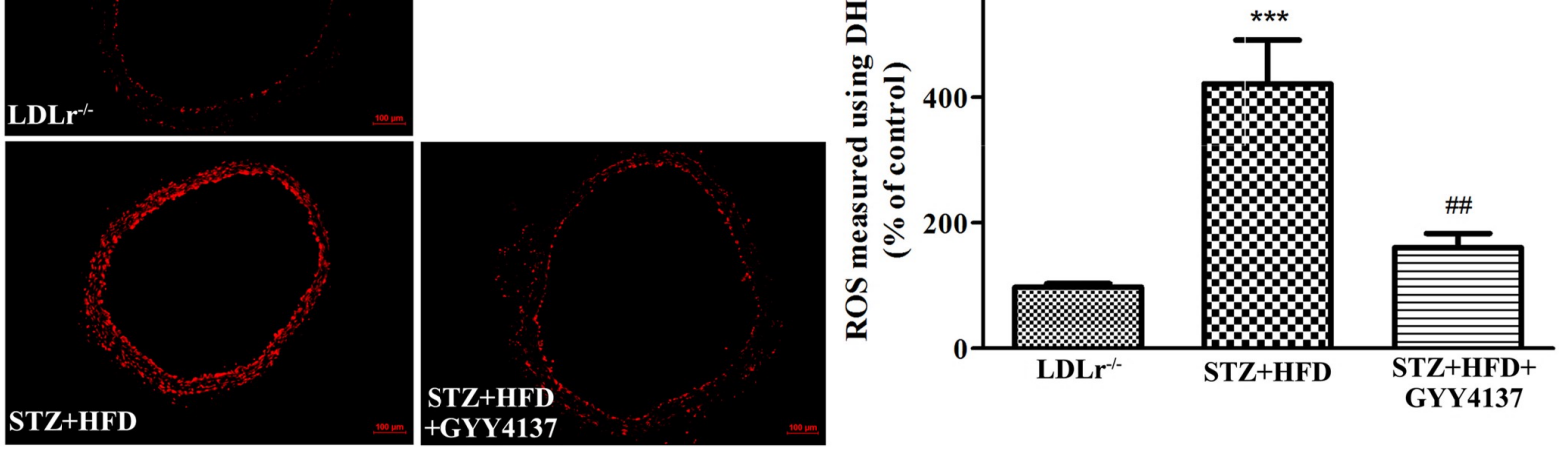
LDLr-/-
STZ+HFD
STZ+HFD
+GYY4137
ROS measured using DH
(% of control)
400
200
0
***
##
LDLr-/-
STZ+HFD
STZ+HFD+
GYY4137

C

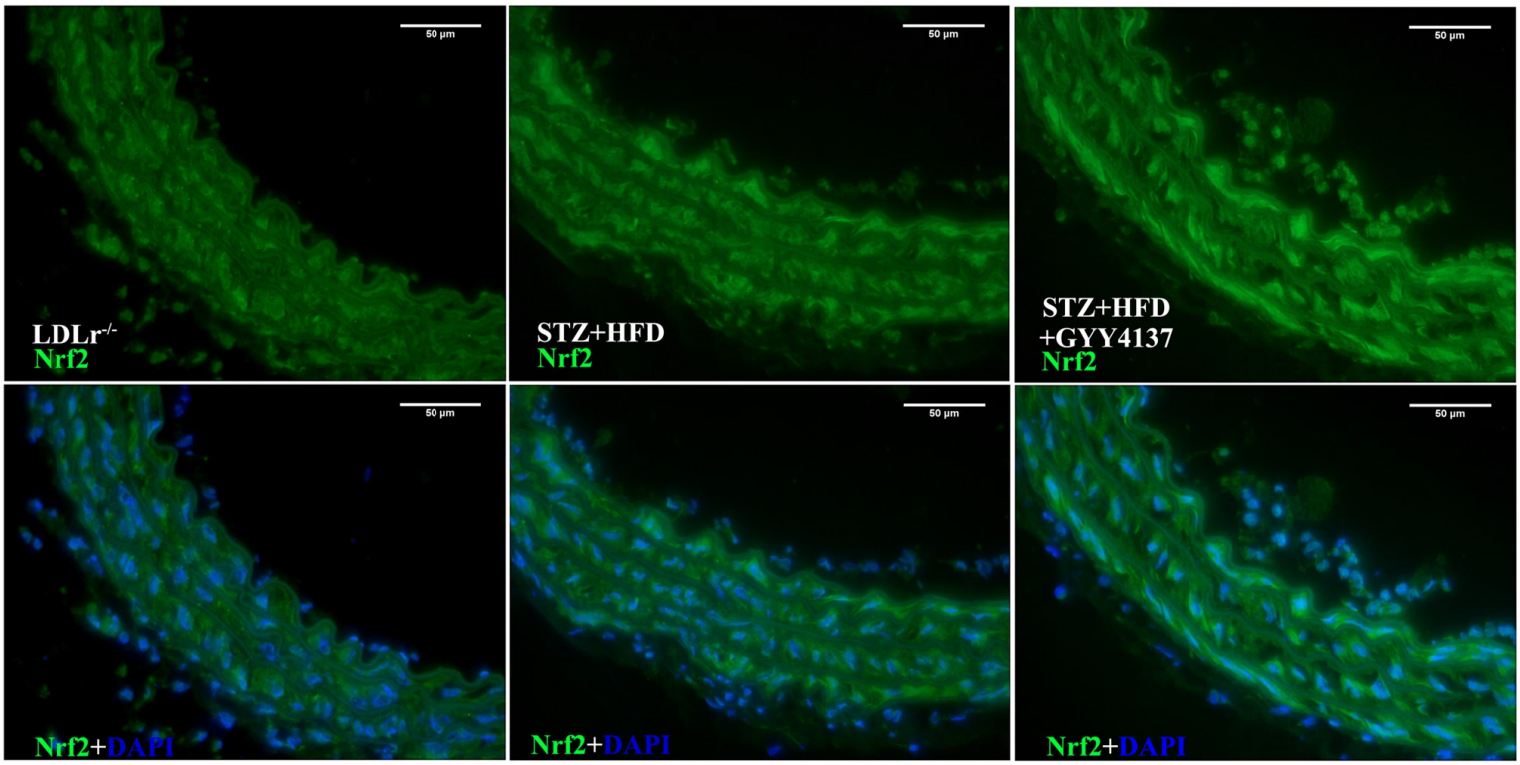
LDLr-/-
Nrf2
STZ+HFD
Nrf2
STZ+HFD
+GYY4137
Nrf2
Nrf2+DAPI
Nrf2+DAPI
Nrf2+DAPI

D

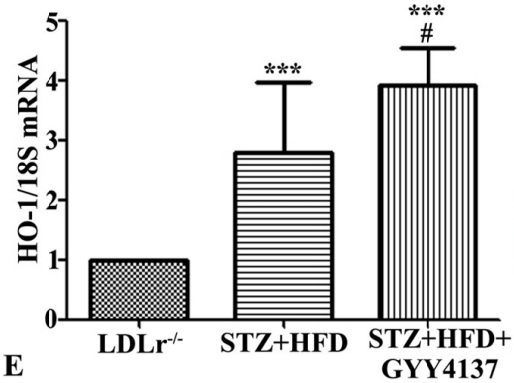
HO-1/18S mRNA
5
4
3
2
1
0
***
***
#
LDLr-/-
STZ+HFD
STZ+HFD+
GYY4137

E

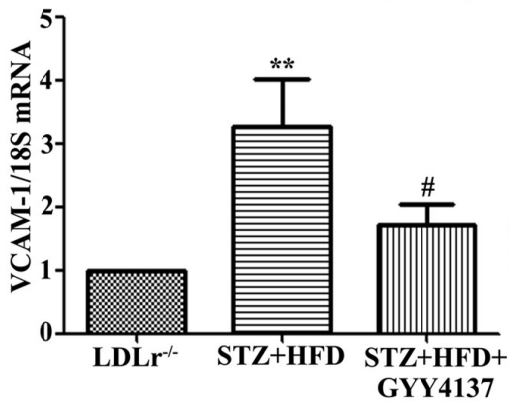
VCAM-1/18S mRNA
5
4
3
2
1
0
**
#
LDLr-/-
STZ+HFD
STZ+HFD+
GYY4137

F


mRNA
5
4
***

G

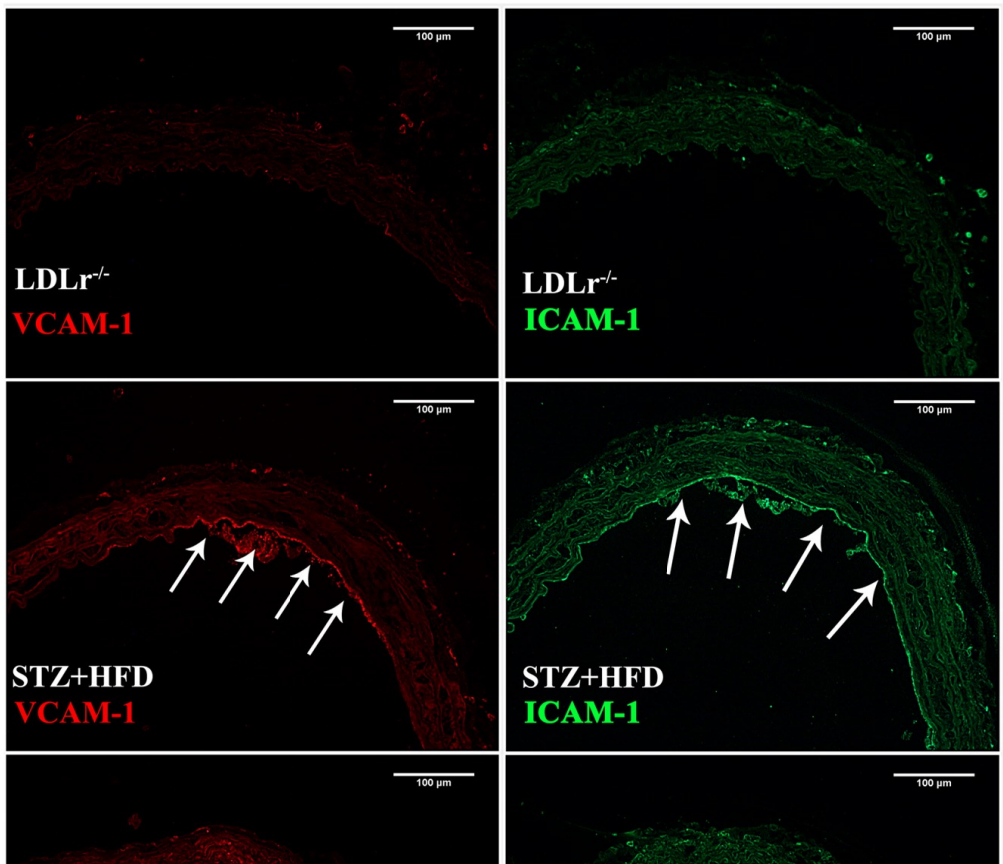
LDLr-/-
VCAM-1
LDLr-/-
ICAM-1
STZ+HFD
VCAM-1
STZ+HFD
ICAM-1

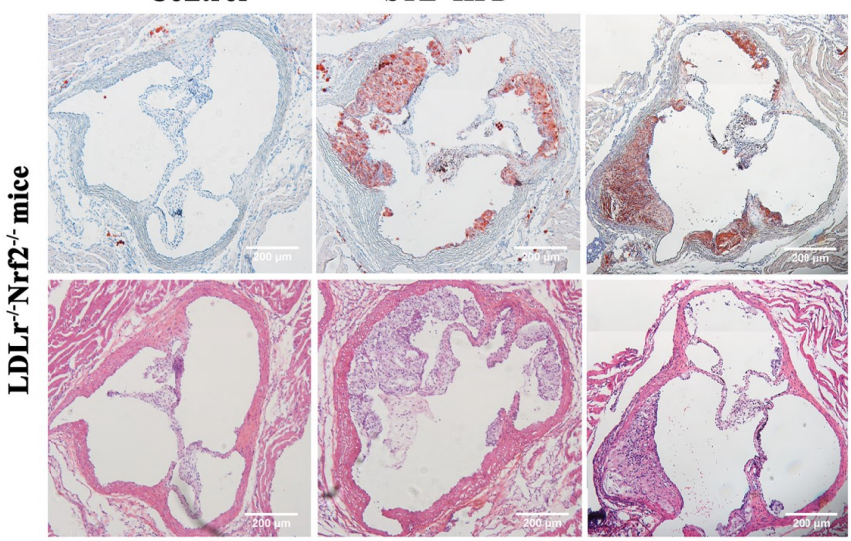
LDLr-/-Nrf2-/- mice
200 μm

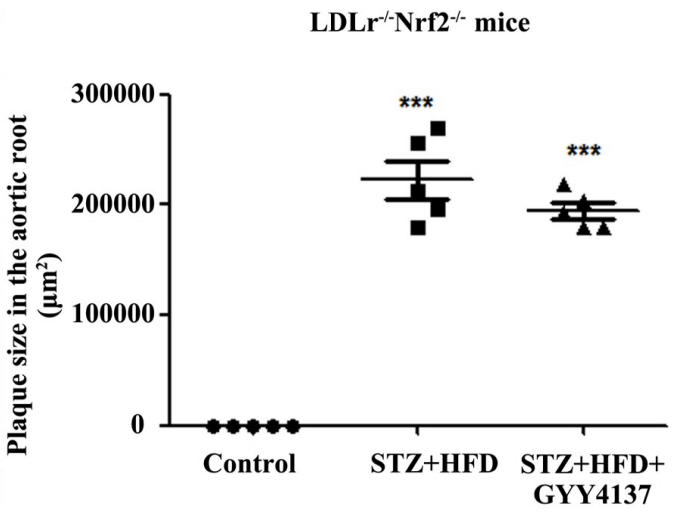
LDLr-/-Nrf2-/- mice
Plaque size in the aortic root (μm2)
300000
200000
100000
0
***
***
Control
STZ+HFD
STZ+HFD+ GYY4137

C

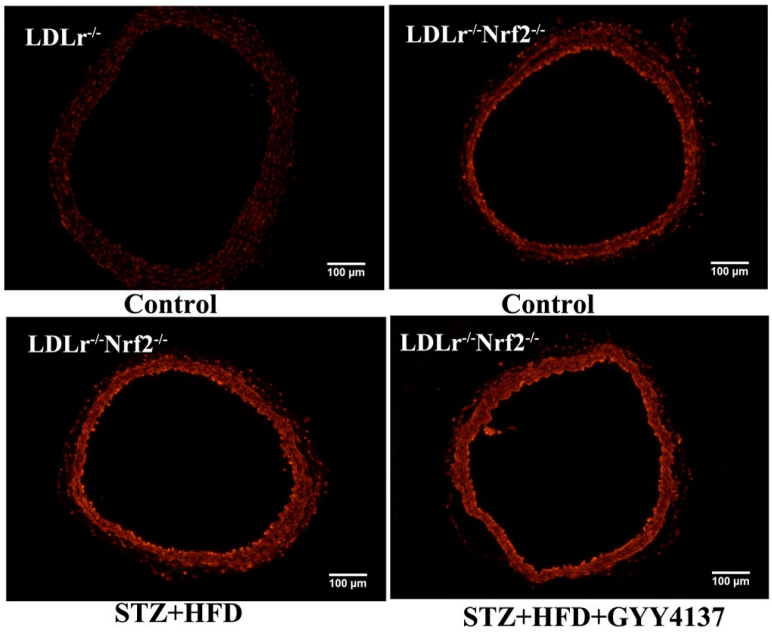
LDLr-/-
LDLr-/-Nrf2-/-
Control
Control
LDLr-/-Nrf2-/-
LDLr-/-Nrf2-/-
STZ+HFD
STZ+HFD+GYY4137
100 μm

D

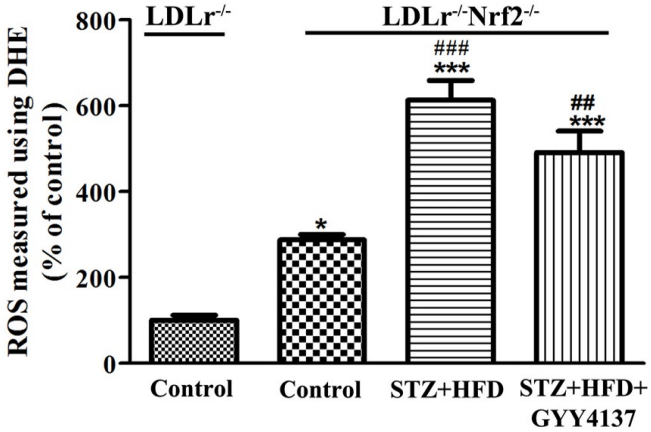
LDLr-/-
LDLr-/-Nrf2-/-
ROS measured using DHE (% of control)
800
600
400
200
0
*
###
***
##
***
Control
Control
STZ+HFD
STZ+HFD+ GYY4137

E

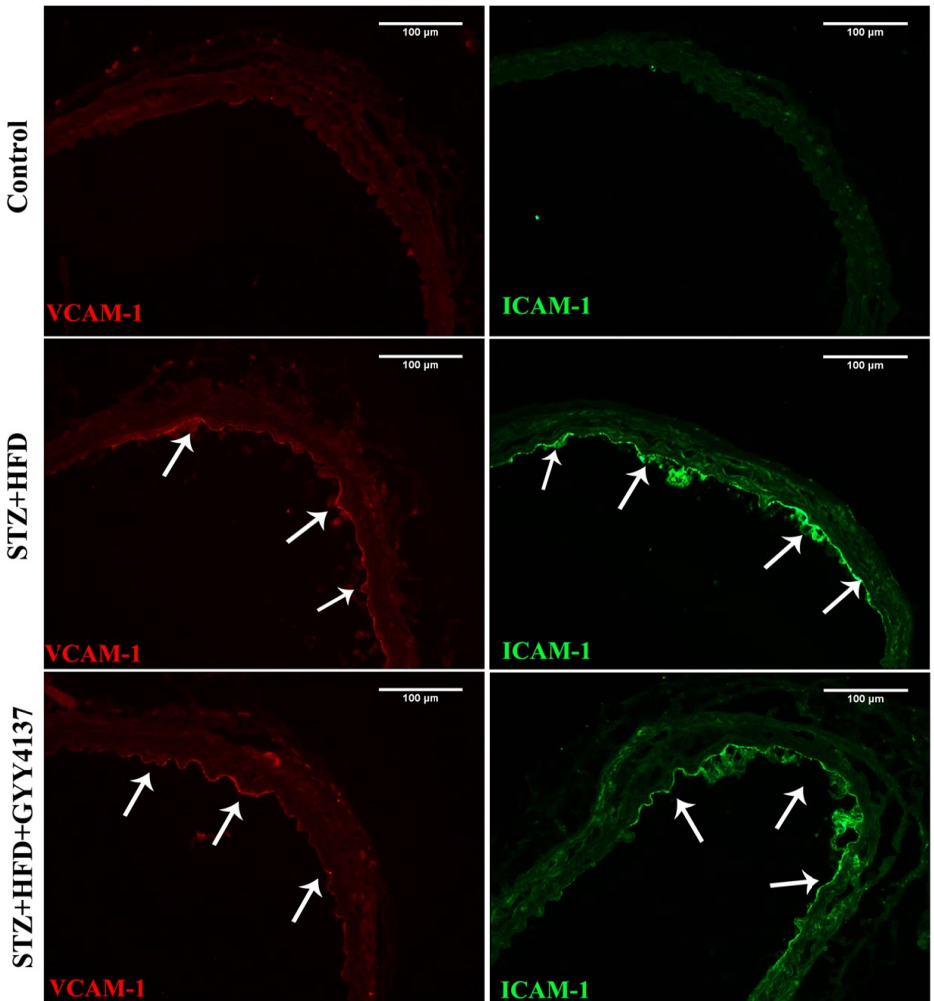
Control
STZ+HFD
STZ+HFD+GYY4137
VCAM-1
ICAM-1
100 μm

F

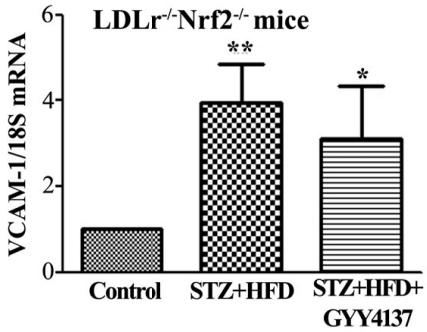
LDLr-/-Nrf2-/- mice
VCAM-1/18S mRNA
6
4
2
0
**
*
Control
STZ+HFD
STZ+HFD+ GYY4137

G

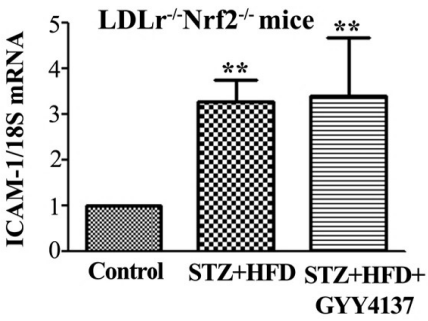
LDLr-/-Nrf2-/- mice
ICAM-1/18S mRNA
5
4
3
2
1
0
**
**
Control
STZ+HFD
STZ+HFD+ GYY4137

H

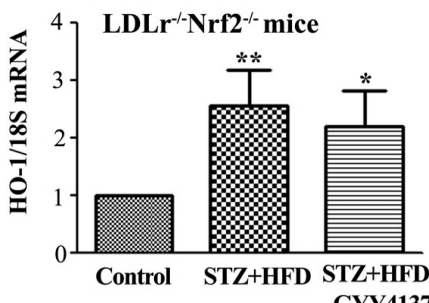
LDLr-/-Nrf2-/- mice
HO-1/18S mRNA
4
3
2
1
0
**
*
Control
STZ+HFD
STZ+HFD+

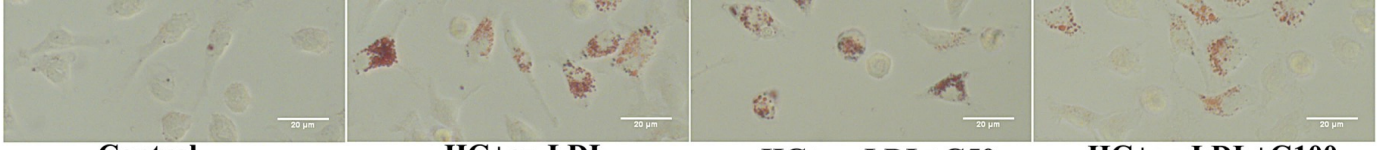
Control
HG+ox-LDL
HG+ox-LDL+G50
HG+ox-LDL+G100

B

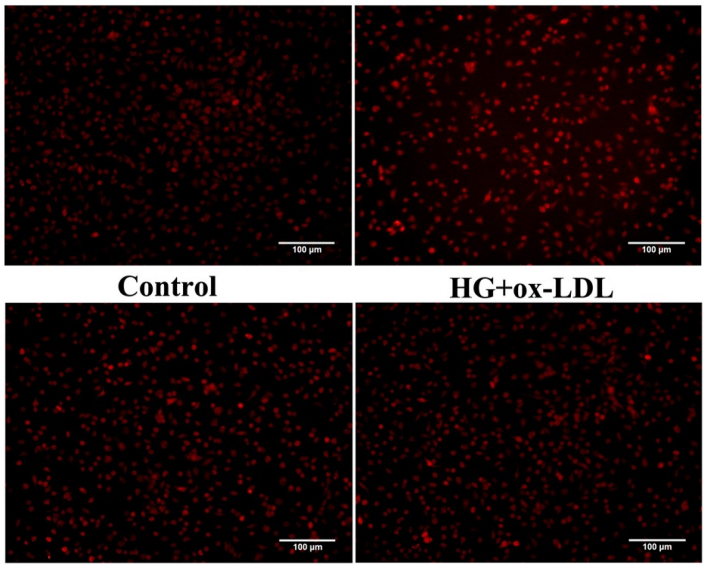
Control
HG+ox-LDL
HG+ox-LDL+G50
HG+ox-LDL+G100

C

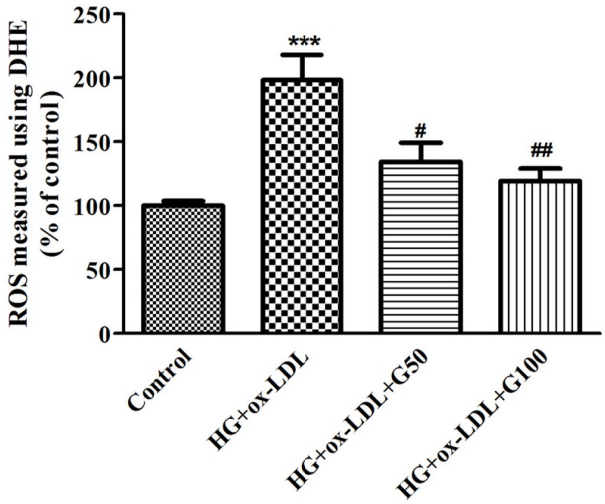
ROS measured using DHE
(% of control)
250
200
150
100
50
0
***
#
##
Control
HG+ox-LDL
HG+ox-LDL+G50
HG+ox-LDL+G100

D

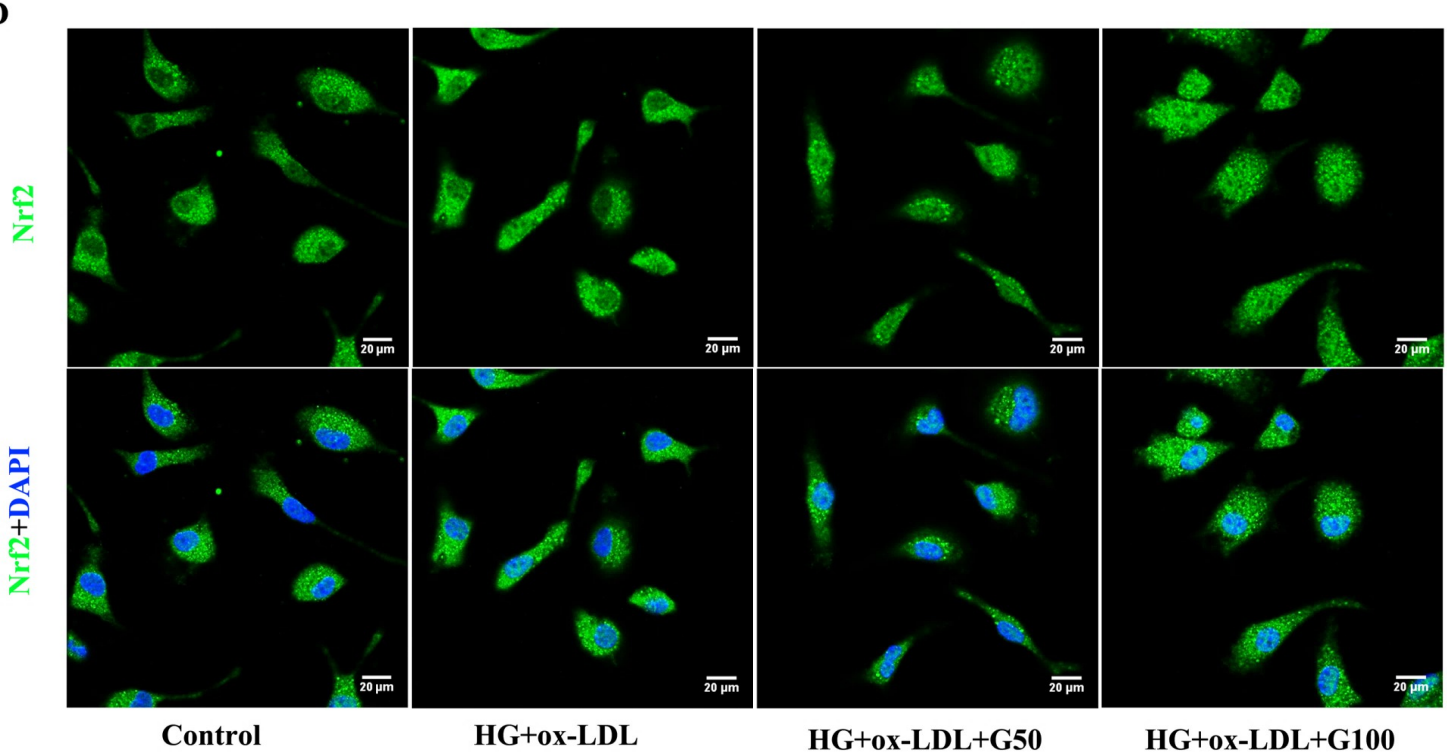
Nrf2
Nrf2+DAPI
Control
HG+ox-LDL
HG+ox-LDL+G50
HG+ox-LDL+G100

E

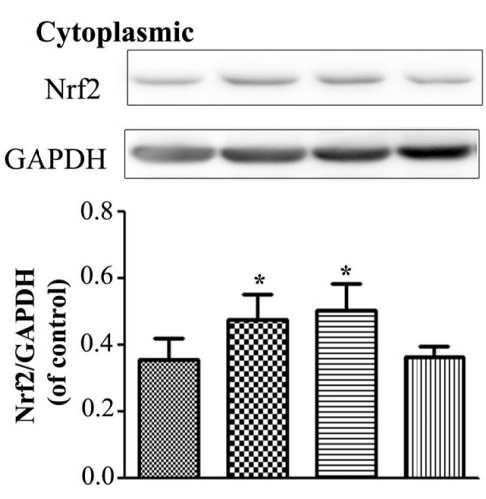
Cytoplasmic
Nrf2
GAPDH
Nrf2/GAPDH
(of control)
0.8
0.6
0.4
0.2
0.0
*
*

F

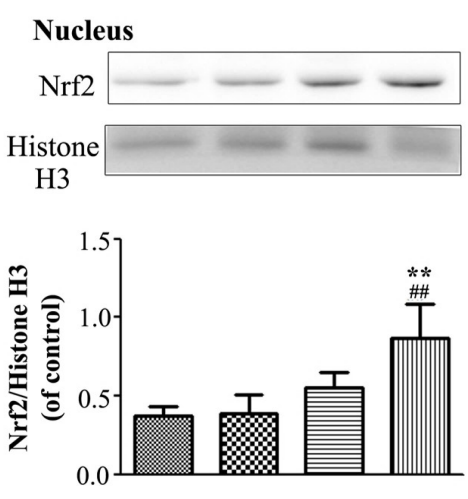
Nucleus
Nrf2
Histone
H3
Nrf2/Histone H3
(of control)
1.5
1.0
0.5
0.0
**
##

G

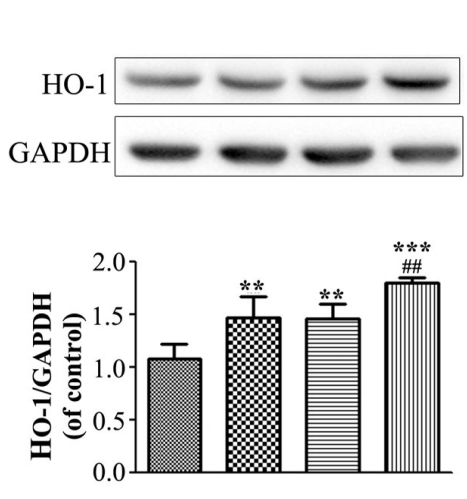
HO-1
GAPDH
HO-1/GAPDH
(of control)
2.0
1.5
1.0
0.5
0.0
**
**
***
##

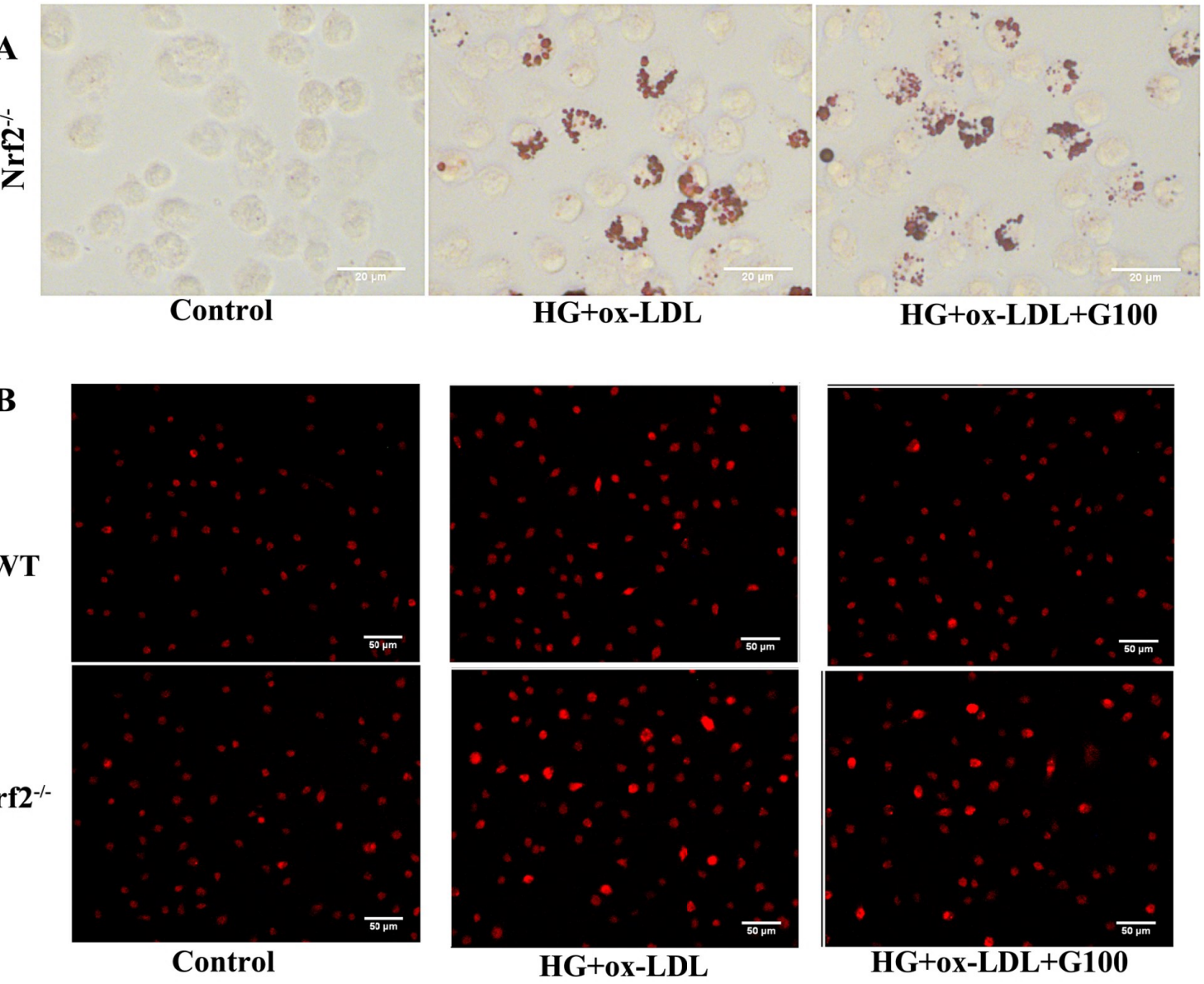
A
Nrf2-/-
20 μm
Control
HG+ox-LDL
HG+ox-LDL+G100
B
WT
rf2-/-
50 μm
Control
HG+ox-LDL
HG+ox-LDL+G100

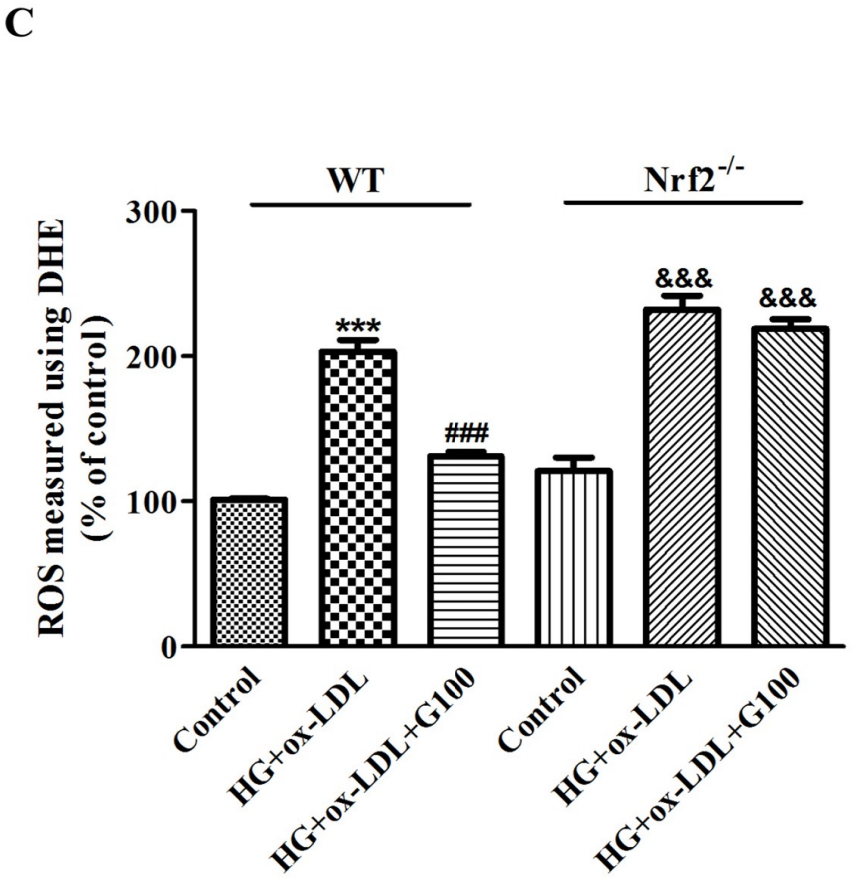
C
WT
Nrf2-/-
ROS measured using DHE
(% of control)
300
200
100
0
***
###
&&&
&&&
Control
HG+ox-LDL
HG+ox-LDL+G100
Control
HG+ox-LDL
HG+ox-LDL+G100

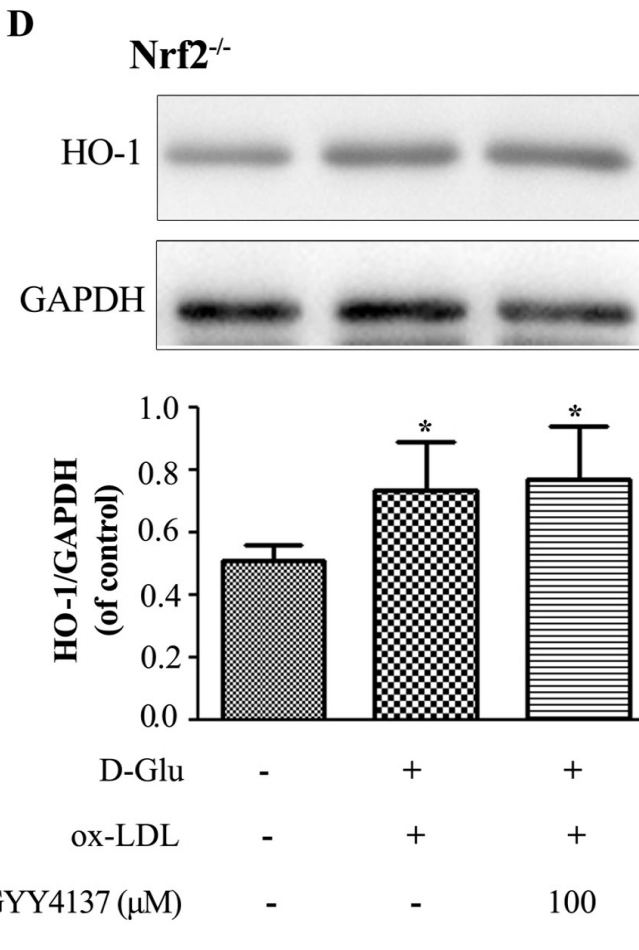
D
Nrf2-/-
HO-1
GAPDH
HO-1/GAPDH
(of control)
1.0
0.8
0.6
0.4
0.2
0.0
*
*
D-Glu - + +
ox-LDL - + +
GYY4137 (μM) - - 100

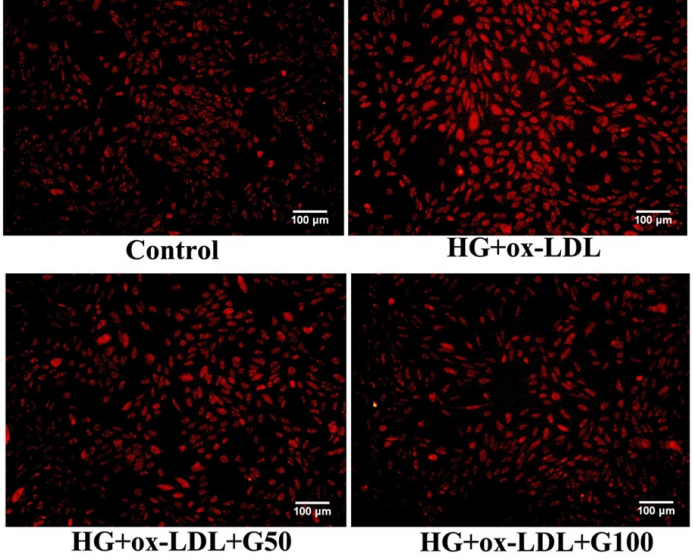
100 μm
Control
HG+ox-LDL
HG+ox-LDL+G50
HG+ox-LDL+G100

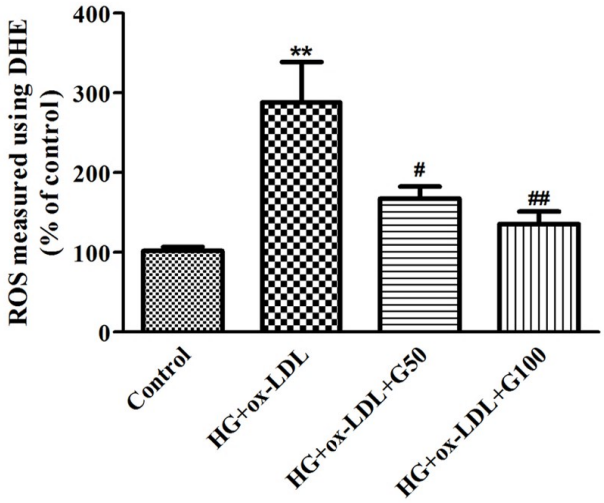
ROS measured using DHE
(% of control)
400
300
200
100
0
**
#
##
Control
HG+ox-LDL
HG+ox-LDL+G50
HG+ox-LDL+G100

C

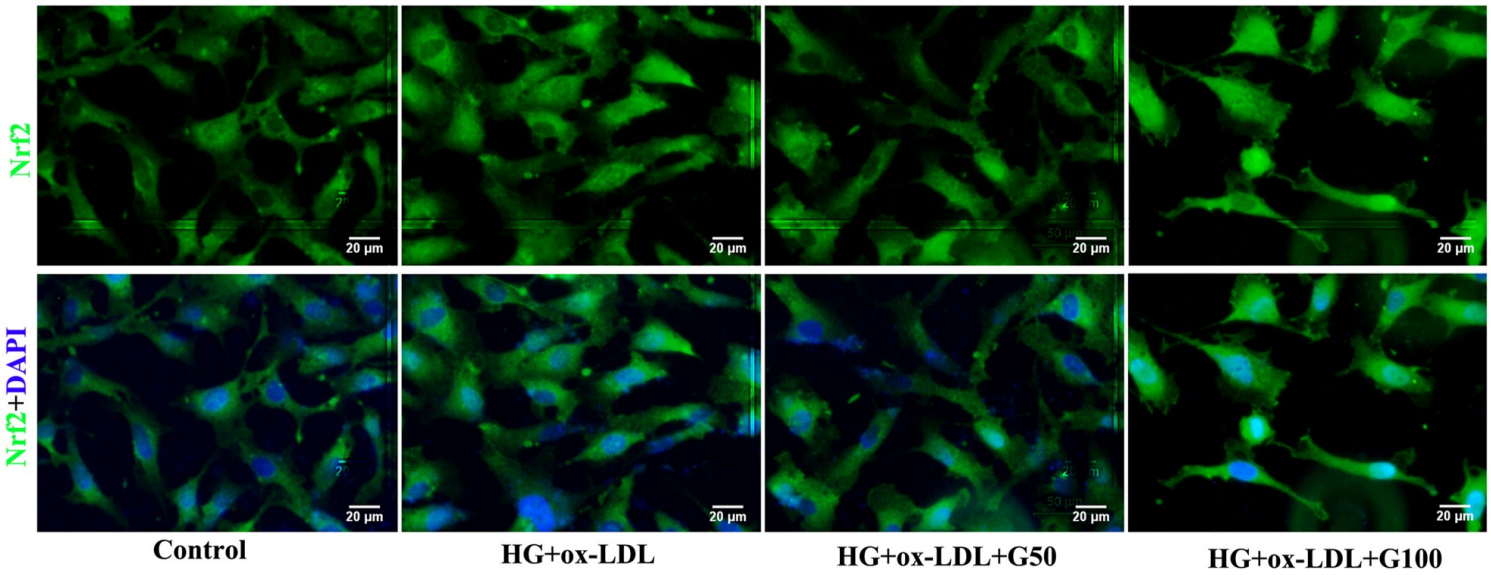
Nrf2
Nrf2+DAPI
20 μm
Control
HG+ox-LDL
HG+ox-LDL+G50
HG+ox-LDL+G100

D

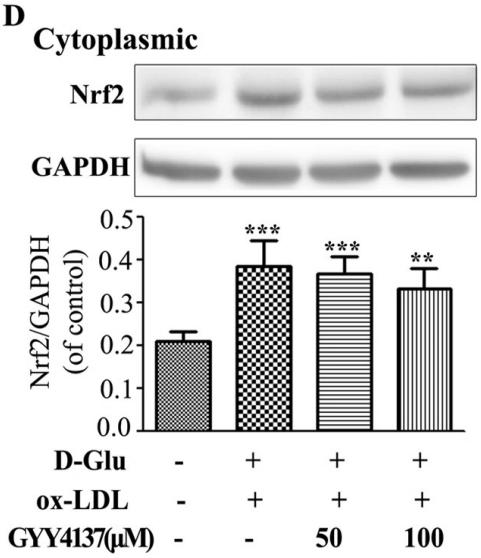
Cytoplasmic
Nrf2
GAPDH
Nrf2/GAPDH
(of control)
0.5
0.4
0.3
0.2
0.1
0.0
***
***
**
D-Glu - + + +
ox-LDL - + + +
GYY4137(μM) - - 50 100

E

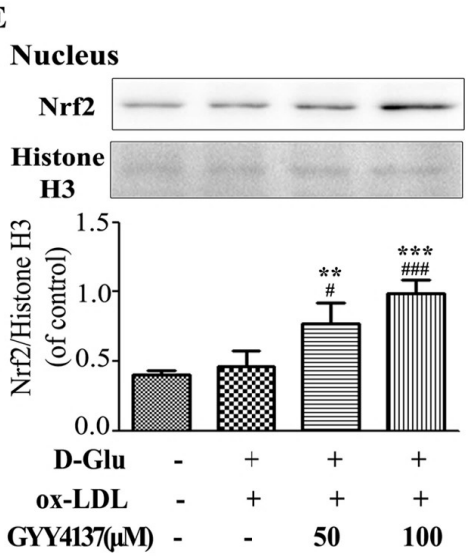
Nucleus
Nrf2
Histone
H3
Nrf2/Histone H3
(of control)
1.5
1.0
0.5
0.0
**
#
***
###
D-Glu - + + +
ox-LDL - + + +
GYY4137(μM) - - 50 100

F

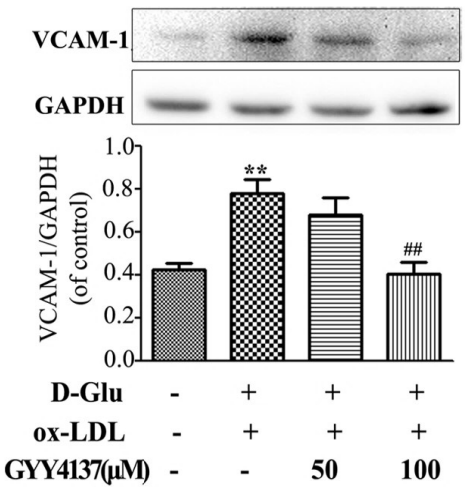
VCAM-1
GAPDH
VCAM-1/GAPDH
(of control)
1.0
0.8
0.6
0.4
0.2
0.0
**
##
D-Glu - + + +
ox-LDL - + + +
GYY4137(μM) - - 50 100

G

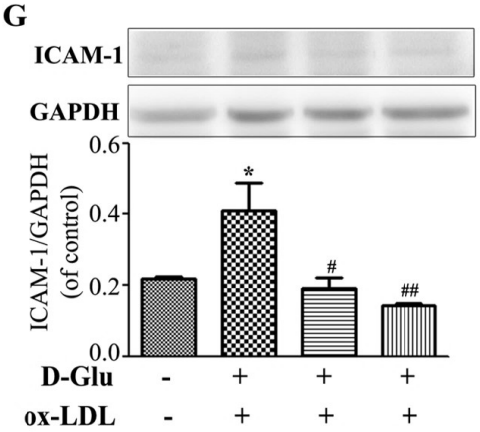
ICAM-1
GAPDH
ICAM-1/GAPDH
(of control)
0.6
0.4
0.2
0.0
*
#
##
D-Glu - + + +
ox-LDL - + + +

H

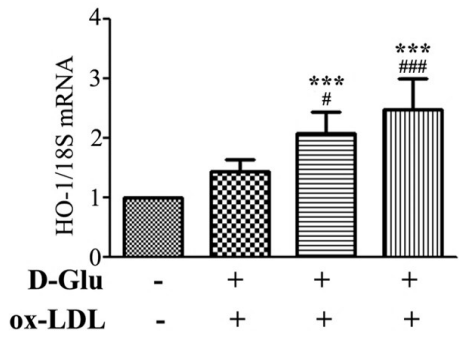
HO-1/18S mRNA
4
3
2
1
0
***
#
***
###
D-Glu - + + +
ox-LDL - + + +

I

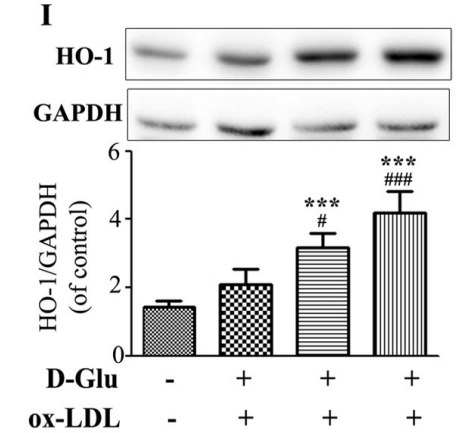
HO-1
GAPDH
HO-1/GAPDH
(of control)
6
4
2
0
***
#
***
###
D-Glu - + + +
ox-LDL - + + +

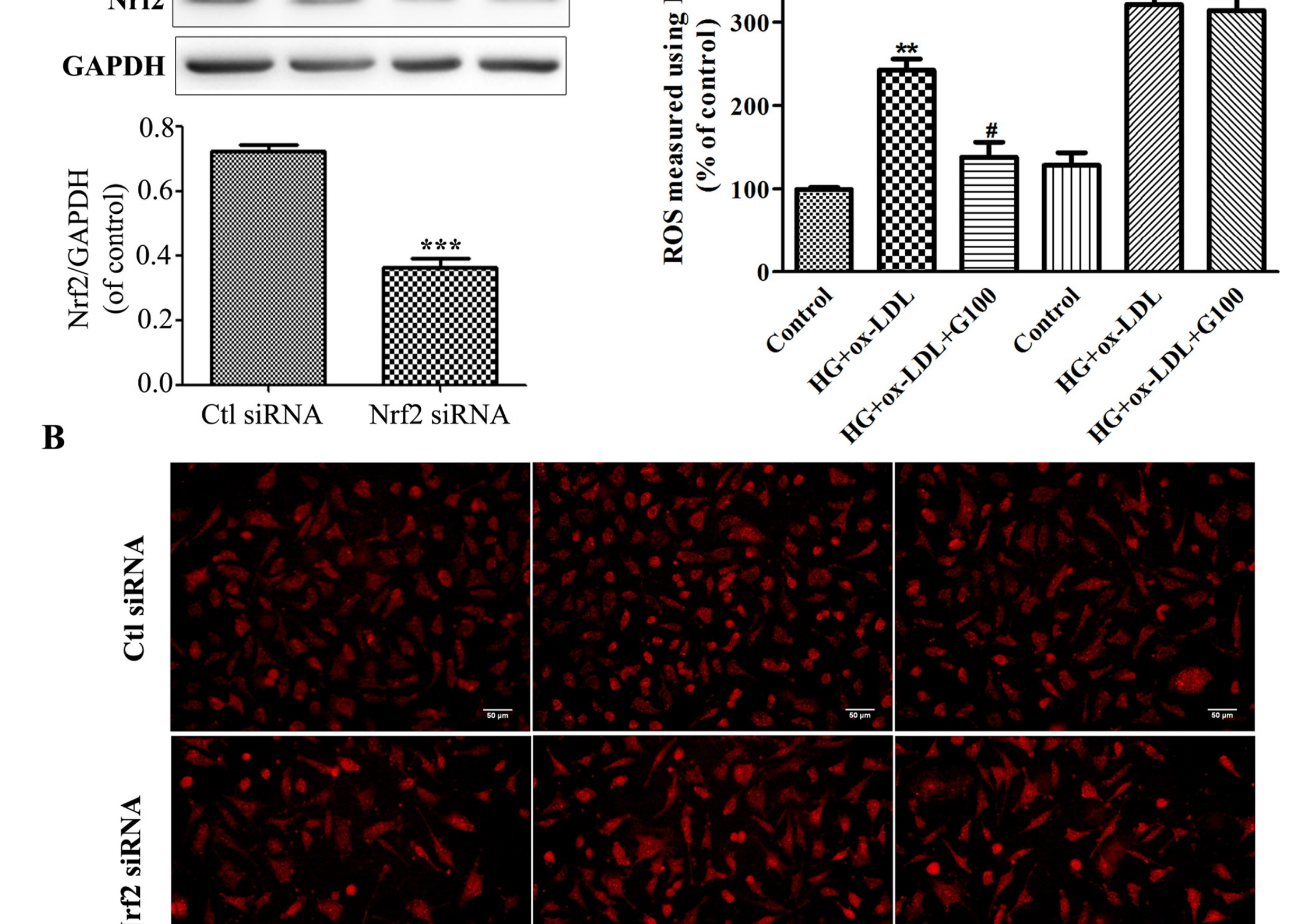
Nrf2
GAPDH
Nrf2/GAPDH (of control)
0.8
0.6
0.4
0.2
0.0
***
Ctl siRNA
Nrf2 siRNA
ROS measured using DCFH-DA (% of control)
300
200
100
0
**
#
Control
HG+ox-LDL
HG+ox-LDL+G100
Control
HG+ox-LDL
HG+ox-LDL+G100
B
Ctl siRNA
Nrf2 siRNA
50 μm
50 μm
50 μm

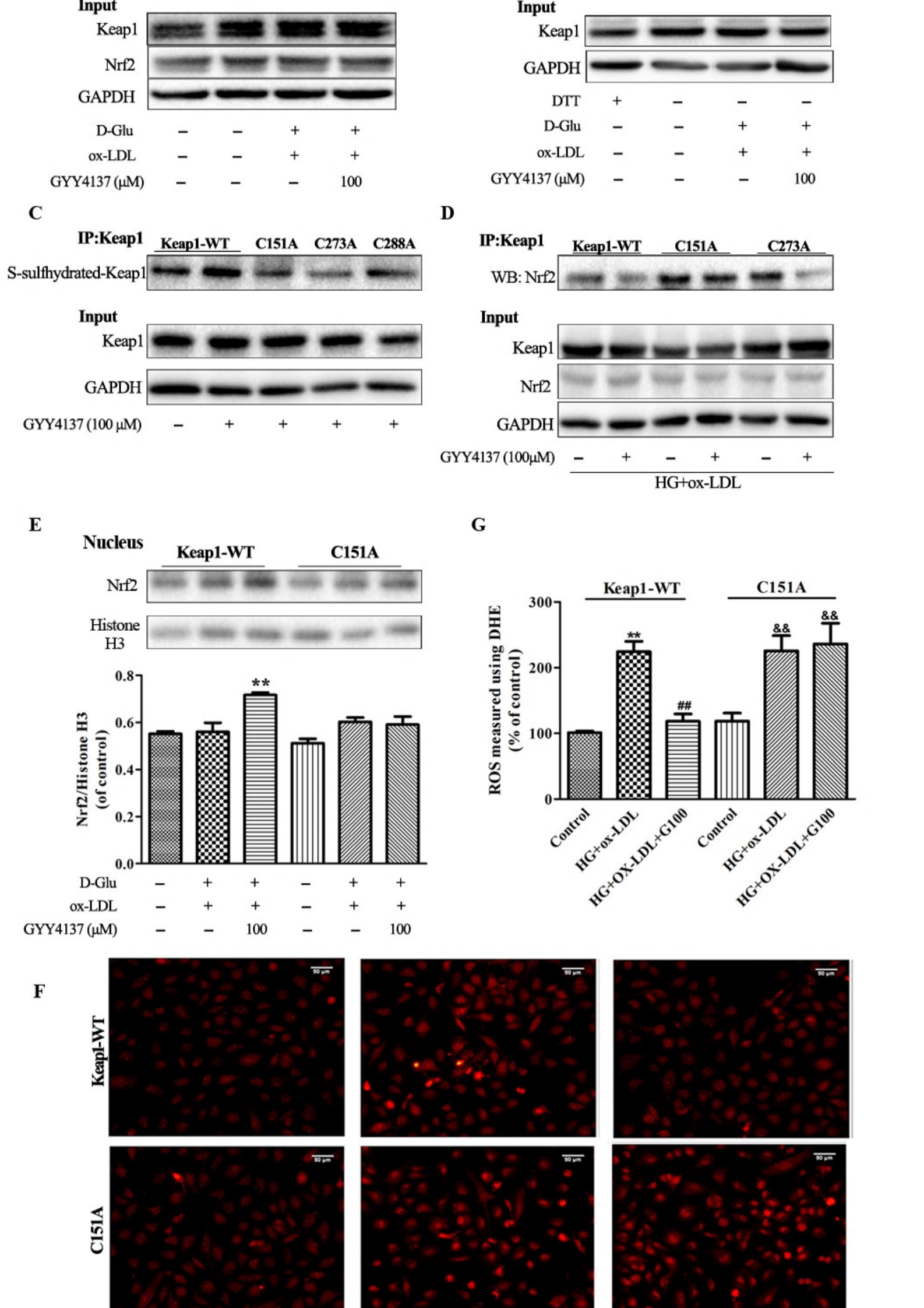
Input
Keap1
Nrf2
GAPDH
D-Glu – – + +
ox-LDL – – + +
GYY4137 (μM) – – – 100
Input
Keap1
GAPDH
DTT + – – –
D-Glu – – + +
ox-LDL – – + +
GYY4137 (μM) – – – 100
C
IP:Keap1
Keap1-WT C151A C273A C288A
S-sulfhydrated-Keap1
Input
Keap1
GAPDH
GYY4137 (100 μM) – + + + +
D
IP:Keap1
Keap1-WT C151A C273A
WB: Nrf2
Input
Keap1
Nrf2
GAPDH
GYY4137 (100μM) – + – + – +
HG+ox-LDL
E
Nucleus
Keap1-WT C151A
Nrf2
Histone H3
Nrf2/Histone H3 (of control)
0.0 0.2 0.4 0.6 0.8
**
D-Glu – + + – + +
ox-LDL – + + – + +
GYY4137 (μM) – – 100 – – 100
G
Keap1-WT C151A
ROS measured using DHE (% of control)
0 100 200 300
** ## && &&
Control
HG+ox-LDL
HG+OX-LDL+G100
Control
HG+ox-LDL
HG+OX-LDL+G100
F
Keap1-WT
C151A
50 μm